

Geo-Congress 2026

GSP 376

Soil Properties, Modeling, and Computational Geomechanics

Selected Papers from Geo-Congress 2026
Salt Lake City, Utah | March 9–12, 2026

Edited by
Jack Montgomery, Ph.D., P.E.
Brady R. Cox, Ph.D., P.E.

ASCE
G-I GEO-INSTITUTE ASCE

GEOTECHNICAL SPECIAL PUBLICATION NO. 376

GEO-CONGRESS 2026

SOIL PROPERTIES, MODELING, AND COMPUTATIONAL GEOMECHANICS

SELECTED PAPERS FROM SESSIONS OF GEO-CONGRESS 2026

March 9–12, 2026
Salt Lake City, Utah

SPONSORED BY

The Geo-Institute
of the American Society of Civil Engineers

EDITED BY
Jack Montgomery, Ph.D., P.E.
Brady R. Cox, Ph.D., P.E.

Published by the American Society of Civil Engineers

Published by American Society of Civil Engineers
1801 Alexander Bell Drive
Reston, Virginia, 20191-4382
www.asce.org/publications | ascelibrary.org

Any statements expressed in these materials are those of the individual authors and do not necessarily represent the views of ASCE, which takes no responsibility for any statement made herein. No reference made in this publication to any specific method, product, process, or service constitutes or implies an endorsement, recommendation, or warranty thereof by ASCE. The materials are for general information only and do not represent a standard of ASCE, nor are they intended as a reference in purchase specifications, contracts, regulations, statutes, or any other legal document. ASCE makes no representation or warranty of any kind, whether express or implied, concerning the accuracy, completeness, suitability, or utility of any information, apparatus, product, or process discussed in this publication, and assumes no liability therefor. The information contained in these materials should not be used without first securing competent advice with respect to its suitability for any general or specific application. Anyone utilizing such information assumes all liability arising from such use, including but not limited to infringement of any patent or patents.

ASCE and American Society of Civil Engineers—Registered in U.S. Patent and Trademark Office.

Photocopies and permissions. Permission to photocopy or reproduce material from ASCE publications can be requested by sending an e-mail to permissions@asce.org or by locating a title in ASCE's Civil Engineering Database (http://cedb.asce.org) or ASCE Library (http://ascelibrary.org) and using the "Permissions" link.

Errata: **Errata, if any, can be found at https://doi.org/10.1061/9780784486719**

Copyright © 2026 by the American Society of Civil Engineers.
All Rights Reserved.
ISBN 978-0-7844-8671-9 (PDF)
Manufactured in the United States of America.

Preface

This is the second volume of seven Geotechnical Special Publications (GSPs) containing papers from Geo-Congress 2026: Geo Tools, Technologies, and Techniques in an Environment of Change, held in Salt Lake City, Utah, on March 9-12, 2026. Notably, this conference marks the 30th anniversary of the Geo-Institute. The conference brought together industry leaders, researchers, and practitioners to showcase innovations, address critical challenges, and advance knowledge in geotechnical engineering. The conference hosted the Terzaghi, Peck, Seed, and Prakash Lectures and many technical sessions, panel sessions, short courses, and student competitions.

These proceedings represent the culmination of nearly two years of effort by the program committee and many other individuals, whose focus has been to continue the success of previous Geo-Congresses and to celebrate 30 years of geotechnical innovation by the Geo-Institute. Building the program started with an international call for papers that resulted in more than 800 abstracts on a variety of important topics. Each paper was subjected to a rigorous technical review by two or more independent peer reviewers. Acceptance required concurrence by at least two peer reviewers, and final decisions were made only after review coordinators confirmed that authors satisfactorily addressed any reviewer comments on their original submission. All accepted papers are presented at the conference as posters or technical talks and are eligible for applicable ASCE awards.

This volume contains a collection of 57 papers focused primarily on the topics of soil properties, numerical and physical modeling, and computational geomechanics. This includes papers on machine learning, laboratory testing, and advanced numerical methods, along with the paper for the 1st Prakash Award and Lecture.

The success of this conference and proceedings would not have been possible without the participation and collaboration of many individuals, including Brad Keelor, the tireless staff at the Geo-Institute, and the many session chairs and reviewers. We hope that these proceedings will be of use to the geotechnical engineering community for many years to come.

The Editors,

Jack Montgomery, Ph.D., P.E., M.ASCE, Auburn University
Brady R. Cox, Ph.D., P.E., M.ASCE, Utah State University

© ASCE

Acknowledgments

We are very grateful for the contributions of the authors, peer reviewers, session chairs, and program committee, without whom this publication would not be possible.

Geo-Congress 2026 Conference Program Committee

Conference Chairs
K. N. Gunalan, Ph.D., P.E., BC.GE, Pres. 20 ASCE, NAC, HNTB Corporation
Ryan B. Maw, P.E., G.E., BC.GE, F.ASCE, Gerhart Cole

Technical Chair
Shideh Dashti, Ph.D., M.ASCE, University of Colorado Boulder

Proceedings Editors
Brady R. Cox, Ph.D., P.E., M.ASCE, Utah State University
Jack Montgomery, Ph.D., P.E., M.ASCE, Auburn University

Student Program Liaison
Cassandra Rutherford, Ph.D., P.E., M.ASCE, Iowa State University

Program Committee Members
Aaron L. Leopold, P.E., M.ASCE, Dan Brown and Associates
Kam Ng, Ph.D., P.E., M.ASCE, University of Wyoming
Jenny Ramirez, Ph.D., P.E., M.ASCE, Geosyntec Consultants

© ASCE

Contents

Shamsher Prakash Award

1st Prakash Lecture: The Influence of Soil Gradation on the Penetration Resistance and Dynamic Response of Level and Sloping Ground 1
Jason T. DeJong, Alejandro Martinez, Katerina Ziotopoulou, Trevor Carey, and Daniel Wilson

Computational Geotechnics

Development of a Modified Cam-Clay Model for Unsaturated Soils under Elevated Temperatures 24
Toan Duc Cao

Classification of Densely Packed Sand Particles Using a Digital Camera and the Segment Anything Model (SAM) 34
Linzhu Li and Magued Iskander

Comparative Analysis of AI Models for LiDAR and Drone-Based Change Detection in Slope Stability Assessment 45
Suprobha Biswas Darothy, A. Q. M. Zohuruzzaman, and Sadik Khan

Synthetic Datasets and Machine Learning Algorithms for Enhanced Calibration of Plasticity Models for Liquefiable Geosystems 53
Tyler Southam, Maziar Mivehchi, Laura Luna, and Katerina Ziotopoulou

Critical State Behavior of Granular Materials from Direct Shear, Simple Shear, and True Triaxial Discrete Element Simulations 63
Esteban Patino-Marin, Fernando E. Garcia, David G. Zapata-Medina, and Luis G. Arboleda-Monsalve

Cross-Comparison of Plastic Hardening Models in FLAC3D and PLAXIS3D for Soil Behavior Simulation 74
Mehrdad Karimipetanlar, Peter Kottke, and Mahsa Jerdi

Development and Application of Mesh Independent Non-Local Model in FLAC2D 83
Sameer Lawankar, Prasoon Garg, Bhardwaj Pandit, and Gaurav Tiwari

Development of Deep Learning Based Model for Estimating Erosion Rates in Cohesive Soils 95
Hiramani Raj Chimauriya, Nripojyoti Biswas, Anand J. Puppala, and Amit Gajurel

© ASCE

Differentiable Machine Learning in Geotechnical Engineering: A Case Study of Bearing Capacity Prediction of Shallow Foundation on Cohesionless Soils **103**
Jun Xiong and Te Pei

Effect of Friction Packing Limit and Drag Model for Predicting Soil Fluidization Behavior due to Pipeline Leakage **113**
Margi Dave and Ashish Juneja

Effect of Particle Refinement Method Parameters in Discrete Element Method Simulations: Cone Penetration Test Examples **120**
Pingki Datta and T. Matthew Evans

Evaluating Gas Blowout Craters in Permafrost Using the Material Point Method **131**
Yu Zhao, Min Liew, and Zhen Chen

Evaluation of a Numerical Modeling of the Radial Expansion and Axial Loading of a New Bioinspired Deep Foundation in Granular Soil **140**
Mohsen Zamani, Peter Zelkowski, Paola Bandini, and Craig Newtson

Evaluation of Retrogressive Slope Failure in Sensitive Clays under Undrained Conditions with Smoothed Particle Hydrodynamics **149**
Enrique M. del Castillo and Jun Geng

Impact of Fluid Column Collapse on Structures Using Higher-Order MPM **159**
Abdelrahman Alsardi, Alba Yerro, and Christopher Long

Influence of Geometry and Mass Distribution on Penetrator Stability in FEM Simulations of Rapid Penetration in Clay **168**
Boules N. Morkos, Mehdi Omidvar, Stephan Bless, and Magued Iskander

Level Set Discrete Element Method Modeling of Naturally Deposited Sand in Triaxial Compression **180**
Peng Tan and Nicholas Sitar

Machine Learning Based Constitutive Models for Predicting Stress–Strain of Sands **189**
Yasaman Abdolvand and Mohammadhossein Sadeghiamirshahidi

Numerical Modeling of Heat Transfer by High-Voltage Cables around Buried Subsea Pipelines Including Trenching and SGD Heat Flux **198**
Kiarash Jafarzadeh and Omid Ghasemi-Fare

© ASCE

Probabilistic Tunnel Collapse Mechanism Based on Smoothed Particle Hydrodynamics and Random Field Theory **208**
Jun Geng, Enrique M. del Castillo, and Ronaldo I. Borja

Seismic Settlement Analysis of Nihal Atakaş Mosque: A Comparison of Field Observations, Empirical and Semi-Empirical Estimates, and 3D Seismic Soil-Structure Interaction Simulation Results **218**
Ozgun Alp Numanoglu, Renmin Pretell, and Daniel Hutabarat

Studying Underground Cavity Progression and the Effects under Levees: A Numerical Investigation Using the Material Point Method **229**
Carole Karam, Alba Yerro, and Sukrityranjan Samanta

Soil Properties and Modeling

A Modified Split Hopkinson Pressure Bar for Temperature-Controlled Dynamic Testing of Frozen Sands **240**
Cocou D. R. Aza-Gnandji, Youssef Abouhussien, and Tugce Baser

A Practical Correlation for Axial Strain at Failure in Drained Triaxial Compression of Sands **250**
Miguel A. Pando and Youngjin Park

A Study of Laboratory Compaction Methods for Foamed Glass Aggregate **261**
Shafkat Bin Jafar, Haifang Wen, Michael P. McGuire, and Tuncer Edil

AI-Powered Rapid Evaluation Scheme for Multiscale Properties of Porous Civil Engineering Materials: Integrating RGB Imaging, Voronoi Random Finite Element (VrFEM), and Numerical Virtual Experiments **271**
Yusheng (Bear) Jiang, Xiong (Bill) Yu, Sreelakshmi Sreeharan, Kiranmayee Madhusudhan, and Hui (Jack) Wang

An Experimental Investigation on Solar Panel (H-Shape Steel) Pile and Frozen Soil Interaction **282**
Zihao Shang, Leela Krishna Mohan Radarapu, Chang Huang, Jeffrey Liu, Alfred Williams, Rohit Pant, and Marcelo Sanchez

An Investigation on the Interactions between Two Root Elements in Sand during Pullout **291**
Sujia Liu, Alejandro Martinez, and Jason DeJong

Analysis of Video Images Obtained during Cone Penetration Testing **301**
Gerald Verbeek and Oksana Khomiak

© ASCE

Application of a Concrete Constitutive Model to Marine Clays Treated with Calcium Carbide Residue 311
Charity Marbaniang and Ashish Juneja

Determining the Preconsolidation Stresses of Low Void Ratio, Highly Overconsolidated Clays 319
Seyed Ahmad Osia and Daniel R. VandenBerge

Effect of Freezing, Drainage Distance, and Radial Location on the Specific Surface Area of Kaolinite Clay 329
Sepehr Akhtarshenas and Sherif L. Abdelaziz

Effect of Strain Rate on Stress–Strain and Pore Pressure Response of Very Soft Clay 338
Shrweta Dutta and Ajanta Sachan

Effect of Undesired Compaction on Hydraulic Properties of Roadside Soils 348
Oguzhan Saltali, Angela Farina, Mikayla Cunningham, Vincent Mwangi, Ahmet H. Aydilek, Allen P. Davis, and Bora Cetin

Evaluating the Influence of Porous Stone Contact Area on Shear Strength Measurements Using a Ring Shear Device 358
Milad Tajik, Yuderka Trinidad González, Casandra Rutherford, and Vernon R. Schaefer

Experimentally Studying the Thermal Sensitivity and Mechanical Response of Kaolin Clay due to Climatic Warming 367
Mohd Sheob, Sarah Aldawood, and Srikanth S. C. Madabhushi

Freezing Curves of Ottawa Sand with Varying Organic Matter and Salinity 376
Junaidul Islam, Tunay Turk, Anshu Abhinav, and Tugce Baser

Harnessing Nitrogen Cycle Reactions to Support the Metabolism of Synthetic Urine for Microbially Induced Carbonate Precipitation of Lunar Soil Simulant 385
Micaela Robson, Marlee Reed, Elizabeth Trubchaninov, Amy Grunden, and Brina Montoya

Image-Based Moisture Content Prediction in Railway Ballast Using Deep Learning 396
Kelin Ding and Erol Tutumluer

Impact of Soil Composition on the Shear Strength of Frozen Soils 407
Hossein Emami Ahari and Beena Ajmera

© ASCE

Impacts of Delayed Inundation during One-Dimensional Consolidation Testing.....416
Asli Acikel, Martin J. Walker, Kevin Stanton, and Robert Chew

Enhancing Soil-Concrete Interface Friction Using a Biomimetic Diamond Snakeskin Texture.....425
Allison Kunz, Jenna Dayley, Kenny Quintana, Kyle M. Rollins, and Taylor J. Sorensen

Influence of Effective Confinement Pressure on Geomechanical Characteristics of Hydrate-Bearing Sediments.....433
Mahima S. Rao, Sahil Wani, and Ramesh Kannan Kandasami

Investigation of the Effect of Pore Water Salinity on the Water Retention Behavior of Bentonite.....443
Mohammadreza Jebeli, Siamak Yoosefi, and Christopher L. Meehan

Lessons Learned in Applying Gravel Interference Corrections for Cone Penetration Test 452
Bret Lingwall and Kody Vandervort

Micro-to-Macro Exploration of Shear Behavior at Sand-Steel Interfaces.....462
Lalit Kandpal, Prashanth Vangla, and Satoshi Matsumura

Non-Invasive Characterization of Soil Moisture Content and Density Using Thermal Imaging, Simulation Modeling, and Machine Learning.....472
Yusheng Jiang, Qingyu Ren, and Hui Wang

Optimization-Based Parameter Calibration of the Hypoplastic Model for Central Florida Hawthorn Group Soils.....482
A. J. Aparicio-Ortube, Luis G. Arboleda-Monsalve, and David G. Zapata-Medina

Particle Size Effects on the Strength of Sand-Structure Interfaces with Snakeskin-Inspired Surfaces.....493
Hyeon Jung Kim and Alejandro Martinez

Physics-Informed Neural Network Approach for Geotechnical Parameter Estimation in Soil Consolidation Analysis.....502
Jin Kim, Jung-Tae Kim, Minshik Rho, Hyun-Joong Hwang, and Gye-Chun Cho

Plant Species Influence on Microbially Induced Carbonate Precipitation: X-Ray Diffraction Analysis of Mineral Formation and Composition.....511
Hannah Hiscott, Pegah Ghasemi, Brina M. Montoya, Celso Castro-Bolinaga, William K. Petry, Amy M. Grunden, Benjamin Breland, and Allison Scates

© ASCE

Preliminary Findings on the Application of mHVSR for Data-Driven Site Response Prediction in California 522
Francisco Javier G. Ornelas, Christopher A. de la Torre, Zhaoting (Steve) Zhang, Tristan E. Buckreis, Scott J. Brandenberg, and Jonathan P. Stewart

Printability and Structural Integrity of Fiber-Reinforced Earth-Based Materials for 3D Printing 532
Suvechha Dhakal and Nitin Tiwari

Residual Strength of Xanthan Gum-Treated Soils 544
Kiran Kuikel, Connor McQuinn, Bernardo Castellanos, and Lucas Walshire

The GeoPoncelet Model for Rapid Penetration in Soils 554
Joseph Thomas Dinotte, Mehdi Omidvar, Stephen Bless, and Magued Iskander

Understanding Soil Spatial Variability and Uncertainty: The Role of Borehole Spatial Distribution in Single Pile Design 565
Fabiana Viscarra, Tommy D. Bounds, and Kanthasamy K. Muraleetharan

© ASCE

1st Prakash Lecture: The Influence of Soil Gradation on the Penetration Resistance and Dynamic Response of Level and Sloping Ground

Jason T. DeJong, F.ASCE[1]; Alejandro Martinez, M.ASCE[2];
Katerina Ziotopoulou, M.ASCE[3]; Trevor Carey, M.ASCE[4]; and Daniel Wilson[5]

[1]Dept. of Civil and Environmental Engineering, Univ. of California, Davis, Davis, CA.
Email: jdejong@ucdavis.edu
[2]Dept. of Civil and Environmental Engineering, Univ. of California, Davis, Davis, CA.
Email: amart@ucdavis.edu
[3]Dept. of Civil and Environmental Engineering, Univ. of California, Davis, Davis, CA.
Email: kziotopoulou@ucdavis.edu
[4]Dept. of Civil and Mineral Engineering, Univ. of Toronto, Toronto, ON, Canada.
Email: trevor.carey@utoronto.ca
[5]Dept. of Civil and Environmental Engineering, Univ. of California, Davis, Davis, CA.
Email: dxwilson@ucdavis.edu

ABSTRACT

Gravelly soils present unique challenges for engineering practice due to the soil becoming more broadly graded and containing relatively large particles. Fundamental changes occur in the soil properties and engineering behavior that make them more challenging to characterize in the laboratory and in situ, evaluate liquefaction triggering, and estimate the consequences on the performance of civil infrastructure (dams, levees, and foundations) when subject to earthquake loading. A systematic research approach that incorporates laboratory experiments, in situ testing, numerical analyses, and physical models is used to produce insights into how soil response may change relative to poorly graded soils, the benchmark granular soil upon which geotechnical engineering practices are largely based. Methods are developed and proposed to account for changes in soil gradation, captured through the coefficient of uniformity (C_u), and the effect of larger particles, captured through the 85th percentile particle size (D_{85}), on soil behavior, penetration resistance, liquefaction triggering, and system deformations. The work presented provides new knowledge and approaches to enable the geotechnical industry to advance the state of practice with respect to well-graded coarse-grained soils.

INTRODUCTION

Evaluating gravelly soils for civil infrastructure such as dams, levees, and foundations, presents a challenge in extending the knowledge base from sandy soils to gravelly soils. As soil becomes more well graded, with increasing percentages of coarser, gravel-sized particles, there are fundamental changes at the particle scale that alter the soil properties and engineering behaviors. These include changes in particle packing and void ratios (index properties), hydraulic conductivity, stiffness and strength, stress-dilatancy, and critical state line (element behavior). These changes directly influence penetration resistance, how liquefaction triggering occurs (pore pressure generation), and the subsequent strains and displacements (cyclic shear strain and volumetric strain accumulation) of the soil at a system scale.

© ASCE

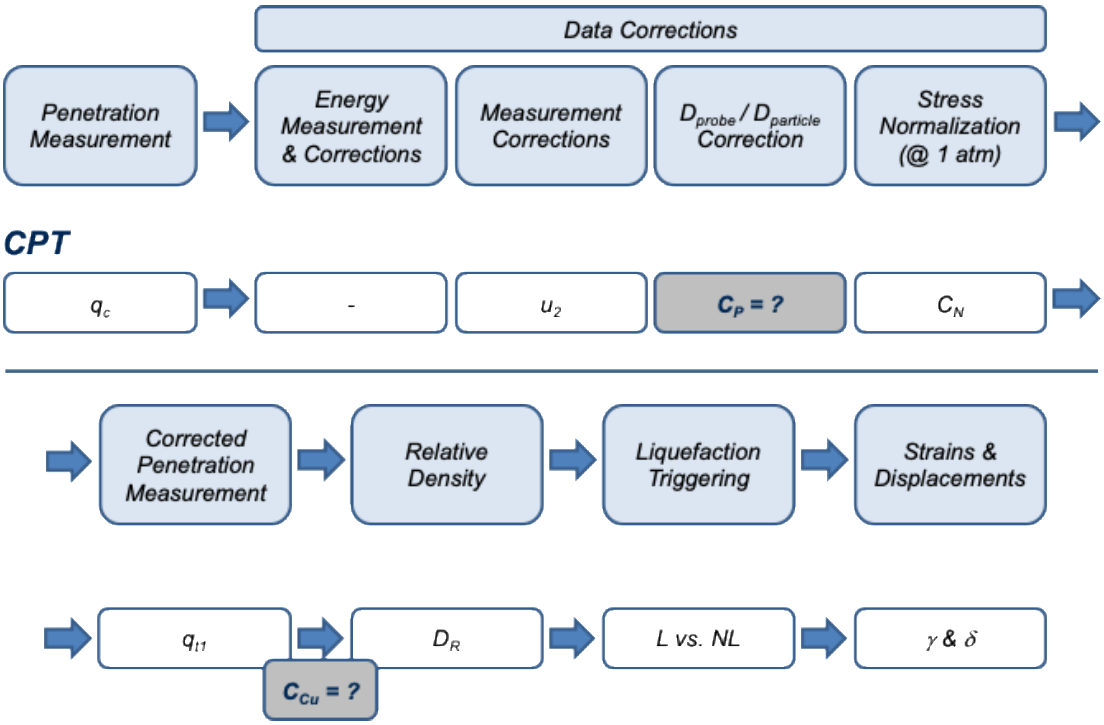


Figure 1. Summary of engineering workflow required for performance-based assessment of soils (blue boxes) and the specific process when the cone penetrometer test (CPT) is used.

The engineering workflow required for the engineering analysis of infrastructure, such as dams, where liquefaction susceptible soils are subjected to earthquake loading includes multiple dependent steps (Figure 1). First, soil characterization includes obtaining an in situ penetration measurement, to which the relevant corrections are applied. This allows for the estimation of initial state by relative density or state parameter, required for the evaluation of liquefaction triggering and prediction of strains and displacements. The composition of gravelly soils, which can be reasonably captured considering the presence of larger particles (e.g. D_{85} representing the 85th percentile particle size, Pires-Sturm and DeJong 2022) and the breadth of the grain size distribution (i.e. coefficient of uniformity, C_u), can impact each of these workflow stages and presents a challenge in accounting and correcting for, respectively, the effect on engineering behavior and analysis processes. Questions arise regarding how the presence of larger particles affects penetration resistance measurements and what correction should be applied, how the effect of soil gradation (C_u) should be incorporated into estimating relative density from penetration resistance, how C_u affects liquefaction triggering (r_u = 1 basis) and post triggering strains and displacements for level and sloping ground in well graded soils relative to poorly graded soils. Herein two terms, one correcting for the influence of large particles on penetration resistance (C_P) and the other accounting for the gradation of the soil (C_{Cu}), are developed and proposed.

The Problem in Practice

Case histories have documented the occurrence of liquefaction in gravelly soils that are very well graded (C_u > 30) and have a hydraulic conductivity comparable to sands (Figure 2). However,

© ASCE

relative to poorly graded soils, there remain challenges and knowledge gaps regarding both the characterization and fundamental behavior of well graded gravelly soils.

For example, measured penetration resistances are typically collected using the Cone Penetration Test (CPT), Standard Penetration Test (SPT), and instrumented Becker Penetration Test (iBPT). These measurements can be elevated due to the larger particles enlarging the failure mechanism (Pires-Sturm et al. 2023). Similarly, measurements of void ratio, density, and stress-strain behavior of well graded soils routinely produce properties that differ from poorly graded soils, but there is a lack of knowledge in how more broadly graded soils differ in their fundamental behavior and uncertainty in how to account for these differences in analyses.

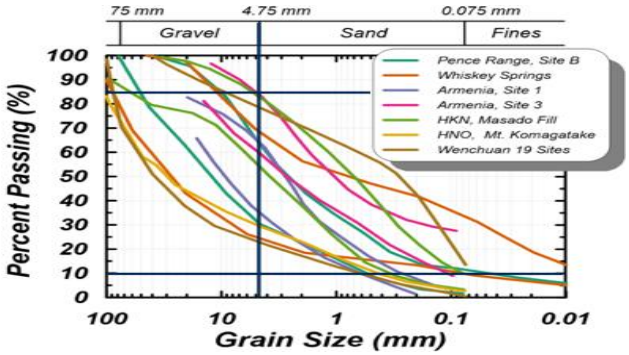


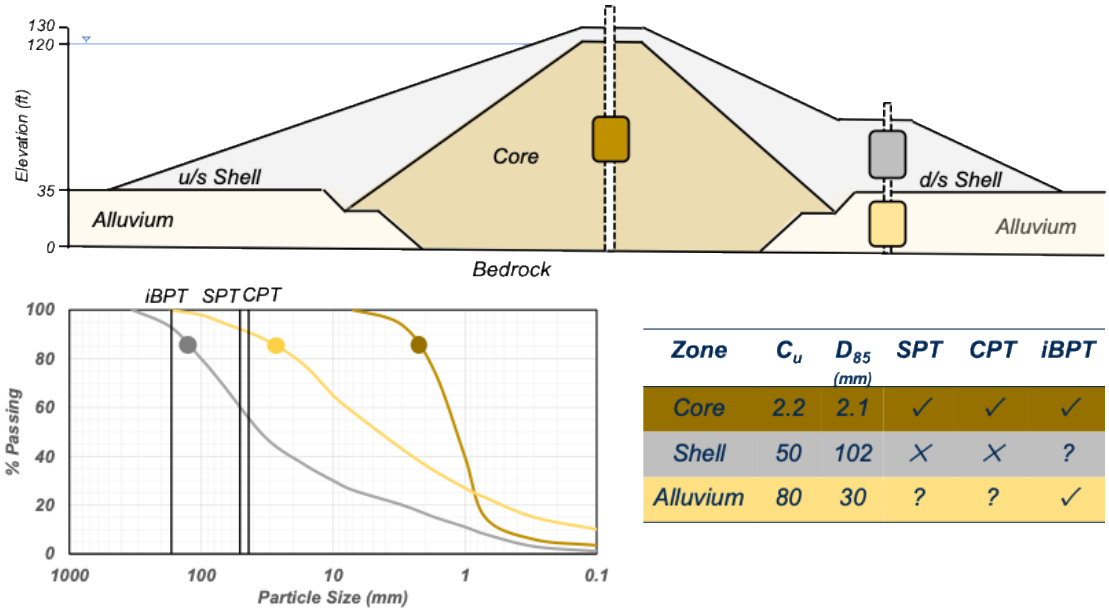
Figure 2. Summary of soil gradation ranges that have liquefied as documented in case histories. Reference lines shown for 4.75 mm particle size as well as for D_{10} and D_{85} thresholds, correlating to percent gravel, permeability, and particle to probe ratio. Adapted from Ghafghazi and DeJong (2016).

Consider the hypothetical, representative, simplified embankment dam in Figure 3, for which liquefaction triggering and deformation analysis is necessary for an updated risk assessment. The dam consists of a silty sand core material with a well graded gravelly shell material and overlying a well graded gravelly alluvium. The soil gradations in the dam vary widely, with C_u up to 80 (Figure 3). There are sufficient smaller particles in all soils, producing sand-like hydraulic conductivity and enabling pore pressure generation during earthquake shaking. There are also sufficient larger particles such that penetration resistance may be compromised due to probe to particle size effects, as large diameter particles are incompatible with the SPT and CPT, and can present a challenge for the iBPT (Figure 3).

Limited guidance exists on probe to particle size effects. The available in situ penetrometers are the SPT (50.8 mm diameter, open-ended, dynamically driven), CPT (43.7 mm diameter, closed-ended, statically pushed), and iBPT (168 mm diameter, closed-ended, dynamically driven, DeJong et al. 2017, Ghafghazi et al. 2017) (Figure 4), which may be used for different parts of the embankment dam depending on the soil properties. Existing literature provides some insight into the applicability of each test. For SPT, the penetration resistance has been found to increase as a function of D_{50} (Kulhawy and Mayne 1990) and gravel content above 20% is likely to produce elevated N values (Mejia via Idriss and Boulanger 2008, Ghafghazi et al. 2017). For CPT, there are fewer and more disparate observations which elevate q_c values when the probe diameter (D_{probe}) to the particle diameter ($D_{particle}$) values are smaller than 20 (Bolton et al. 1999) or 3 (Iqbal 2004). In this scenario, characterization using the iBPT can provide an accurate estimate of an equivalent

© ASCE

the stress normalized clean-sand corrected blow count, $(N_1)_{60\text{-}cs}$, but uncertainty remains in the subsequent engineering analyses.



Zone	C_u	D_{85} (mm)	SPT	CPT	iBPT
Core	2.2	2.1	✓	✓	✓
Shell	50	102	X	X	?
Alluvium	80	30	?	?	✓

Figure 3. Schematic of representative earthen dam cross-section, soil gradations with probe diameters indicated for the iBPT, SPT, and CPT and D_{85} values for the three soils, and a summary table indicating the applicability of the different probes to each soil type (✓ = applicable, X = not applicable, ? = unknown).

Equally, there is not consensus in the literature or practice regarding how broadening of the soil gradation may affect soil properties and engineering behavior. This is due in part to the numerous permutations of soil conditions (e.g. particle size range, gradation range, material hardness, and prepared density, relative density, void ratio, or state parameter) that are possible and to the practical difficulties of performing laboratory and field testing on soils with large particles. Consequently, aggregation of past work is not sufficient to discern first order trends and dependencies, as detailed in Sturm (2019).

Research Approach

While case histories provide important insights regarding performance during earthquakes and help define the problem of interest, the information and data available is insufficient and lacking to develop fundamental insights into the governing mechanisms for the development of robust analysis methods. Consequently, this work uses data from field case histories and site investigation programs in combination with a more structured research study to enable the systematic evaluation of the contribution of soil gradation and particle size to fundamental soil behavior, in situ characterization, liquefaction triggering, and system performance. This was made possible using laboratory tests, numerical analyses, and physical centrifuge models to provide detailed insights. A series of poorly and more broadly graded soils are examined, with as many variables controlled as possible to study the primary parameters of interest, namely gradation and particle size. Further

© ASCE

details about the soils developed are summarized by Pires-Sturm et al. (2023), Sturm (2019), Carey et al. (2022, 2023), and Ahmed et al. (2023). This combined approach produces a clearer understanding of the fundamental mechanisms and enables the development of guidance and methods for practice.



Figure 4. Images of in situ probes relative to USCS soil particle sizes.

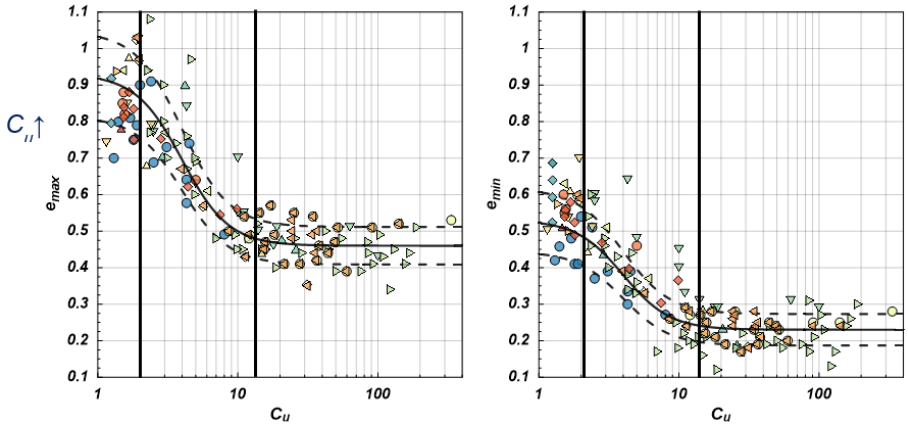


Figure 5. Relationship between C_u with e_{max} and e_{min}. Adapted from Pires-Sturm et al. (2022)

EFFECTS OF SOIL GRADATION (C_u) ON SOIL BEHAVIOR

The coefficient of uniformity, $C_u = D_{60}/D_{10}$, is used to examine the effects of soil gradation on soil behavior. C_u is a simple, easily obtained, and low-cost industry standard metric that effectively captures the broadness of gradation. D_{10} is used because $(D_{10})^2$ is roughly proportional to hydraulic conductivity (k) (Hazen 1911) and D_{85} is useful to evaluate probe to particle size effects (Pires-Sturm and DeJong 2022). It is important to note that the percent gravel was found to not be a reliable metric in this study. This is attributed to the fact that both sand and gravel behaviors are controlled predominantly by effective stress and the gravel size threshold in classification methods

© ASCE

is somewhat arbitrary and variable (e.g., USCS D2487 (2020), BS 5930 (2020)). Instead, as shown herein, the soil's D_{85} and C_u were found to be more robust metrics.

Observations compiled from 159 datasets (Figure 5) including test soils, geologic deposits, and anthropogenic (engineered) soils produce persistent trends that indicate a transition zone in void ratio indices (e_{max} and e_{min}) that can be reasonably modeled with a hyperbolic function (Pires-Sturm et al. 2022). The transition zone occurs primarily from C_u = 2 to 12 during which the void ratio indices reduce by a factor of about 2: e_{max} trends from an average of 0.9 to 0.45 and e_{min} from 0.5 to 0.25. The subsequent leveling off above about C_u = 12 indicates a consistent saturation in packing efficiency, and may indicate that dependent measures, such as soil properties and penetration resistance, could also become less sensitive or saturated at higher C_u values (additional research is needed to confirm this).

A suite of ten test soils of varying C_u and D_{50} were generated from the same natural alluvial deposit so that the secondary parameters (i.e. particle mineralogy, shape) could be held as constant as practically possible. Figure 6a-c provides a selection of these soils and their properties. The fines content is < 5% for all soils and the hydraulic conductivity (k) was intentionally controlled to be similar, so results are independent of k. Two binary, gap-graded mixtures were also evaluated, but their behavior and trends did not map with the smoothly graded soils (Pires-Sturm et al. 2022, Love 2022).

Experimental results revealed the triaxial behavior of the soils, presented in Figures 6d-f (see Ahmed et al. 2023 for further analysis). For a constant relative density (D_R), e decreases as C_u increases. The effect of gradation on soil behavior is not clearly discernable when holding the D_R constant, and instead the state parameter (ξ), as defined by Been and Jefferies (1985), provides more clear trends. As evident in Figures 6d-f, increases in C_u result in greater peak friction angle (ϕ'_{peak}) and dilation angles (ψ) and a leveling of the critical state friction angle (ϕ'_{cs}). For the critical state line, as C_u is increased, lower intercepts (Γ) and flatter slopes (λ) are observed. Peak strength increases significantly and the critical state line becomes progressively flatter due to the void ratio change. This means that below critical state there is stronger dilation, and above critical state there is the potential to generate pore pressures more rapidly. The Bolton (1986) stress dilatancy relationship shown in Figure 7 reveals that across different confining stresses, for any D_R, the difference between the peak and critical state friction angle increases with greater C_u. A clear systematic increase is observed for peak friction angle and dilation rate as C_u increases.

Discrete Element Model (DEM) simulations were calibrated against the laboratory test suite to provide particle-scale insights (Figure 8, Basson et al. 2024). Results confirmed a downward shift and flattening of the critical state lnes and increased dilatancy as C_u increases, and the trends with respect to D_R and initial ξ persist. DEM also allows for investigation of the fabric, revealing that larger particles govern the load transmission and comprise the "strong" contact network. The strong contact network (contact normal force greater than the average) carries most of the load, whereas the weak contact network (contact normal force greater than the average) provide buckling resistance to the strong force network. For poorly graded soils, the fabric becomes anisotropically oriented, with a preference for vertical contacts. However, the fabric anisotropy in well graded soils is considerably greater. These findings indicate that the larger particles in the assembly have higher forces propagating through them than the smaller particles, so the larger particles govern the transfer of load and thus the response during shearing (Kuei et al. 2020, Basson et al. 2024)

Direct simple shear testing on poorly graded and well graded soils reveals how cyclic behavior changes from a C_u 2 to 8 (Figure 9) (Humire 2022, Reardon 2021). While the effect of gradation

© ASCE

on the initial number of cycles to triggering (N_{liq}) is unclear in the literature and requires more investigation, aggregated data shows that N_{liq} either decreases slightly or remains unchanged with increasing C_u. For post-liquefaction triggering, well graded soils require more cycles to reach 10% strain than poorly graded soils and thus have a smaller rate of strain accumulation. The post-triggering volumetric reconsolidation strains also decrease as C_u increases. DEM simulations of cyclic DSS tests reveal that the post-liquefaction decrease in shear strains for the more broadly graded soils are due to the greater number of contacts per particle (i.e., greater particle connectivity) and the smaller fraction of contacts that are sliding at any given moment.

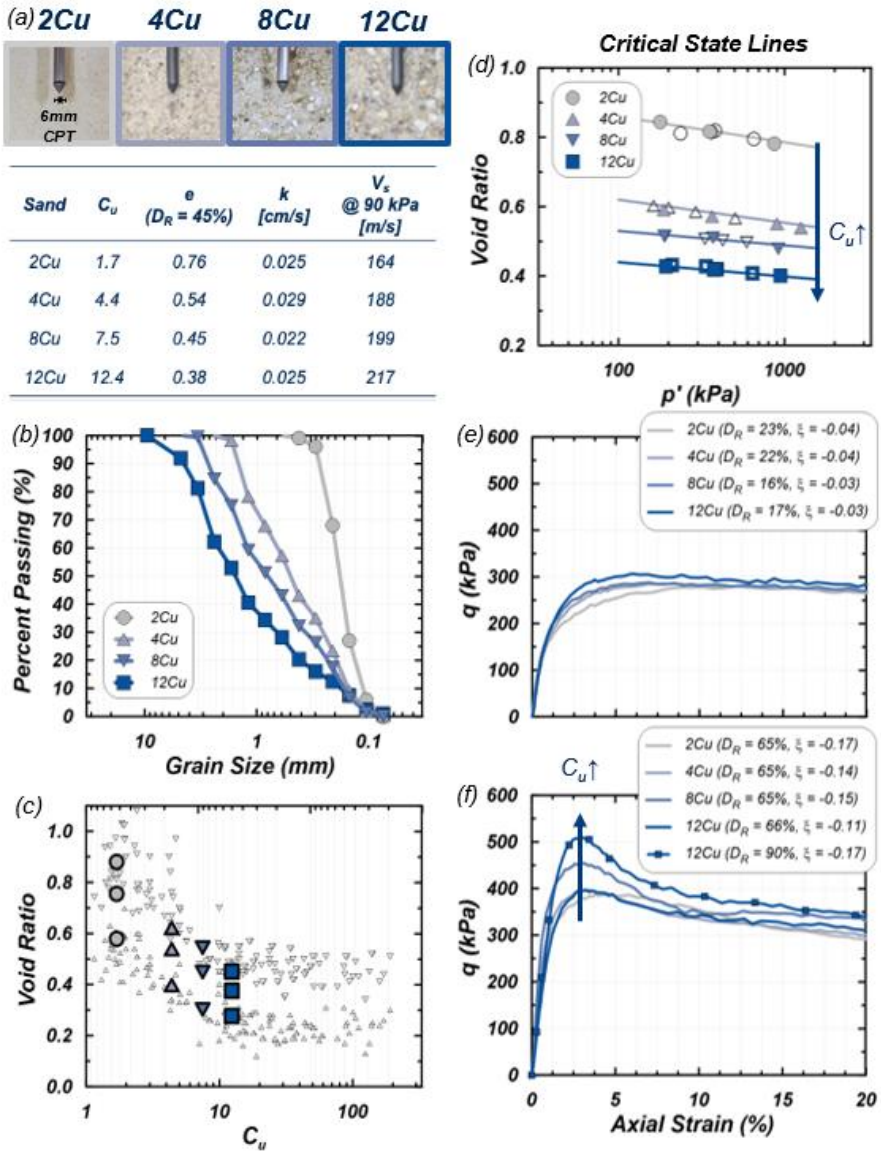


Figure 6. (a) Summary of soil properties, (b) soil gradation, (c) e_{max}, $e_{Dr=40\%}$, and e_{min}, and (d) critical state lines, and drained shear response for (e) loose/contractive and (f) dense/dilative conditions from drained triaxial tests (adapted from Ahmed et al. 2023).

© ASCE

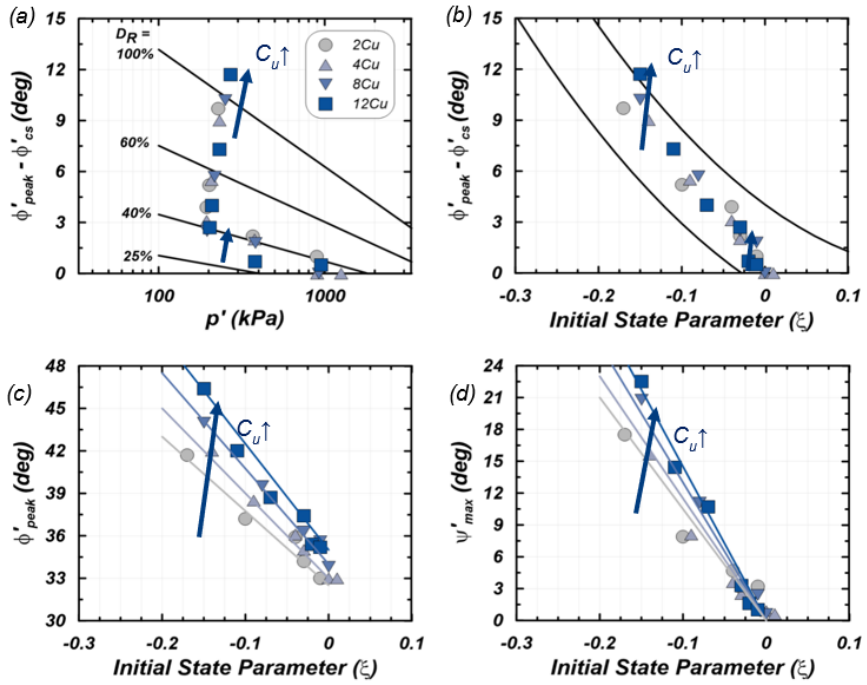


Figure 7. Shearing behavior for ($\phi'_{peak} - \phi'_{cs}$) versus (a) p' and (b) initial state parameter and (c) (ϕ'_{peak}) and (d) ψ'_{max} versus initial state parameter from triaxial tests (adapted from Ahmed et al. 2023).

IN SITU PENETRATION RESISTANCE

Various penetrometers are used for in situ characterization of penetration resistance and relative density following the generalized workflow outlined in Figure 1. The systematic approach presented was developed using CPT data, but is expected to be conceptually applicable to other penetration equipment (e.g. SPT and iBPT). After a penetration measurement is collected, the necessary data corrections are applied to obtain a corrected penetration measurement that can be used to estimate the relative density. For CPT the measurement correction is $q_t = q_c + u(1 + a)$ where u_2 is the pore pressure (shoulder) and a is the tip area ratio. The overburden stress correction from Idriss and Boulanger (2008) is $q_{t1} = C_N q_t$ with $C_N = (P_a/\sigma'_v)^{m_e}$ where m_e was found to be between 0.784 – 0.521D_R in the field and practice (Idriss and Boulanger 2008) and 0.5 to 1.0 in the centrifuge (Pires-Sturm and DeJong 2023)

Penetration data in gravelly soils requires two additional consideration, one correction for the probe to particle size effects and one term to incorporate the influence of soil gradation. The probe to particle size correction, $C_P = f(D_{probe}/D_{particle})$, detailed later, reduces the q_t to that would be obtained if the penetration resistance was obtained with a sufficiently large probe to avoid compromising the penetration mechanism. The coefficient of uniformity term $C_{Cu} = f(C_u)$, detailed later, is not a correction but instead enables systematic incorporation of the effect of soil gradation into subsequent analysis steps. Together these corrections produce a functional form for D_R as follows, where α, β, and γ are calibrated to poorly graded SP sand:

© ASCE

$$D_R = \alpha \left(\frac{q_{t1}}{P_a C_P C_{Cu}} \right)^{\beta} + \gamma \quad (1)$$

To populate and inform Equation 1, experimental data was collected at the UC Davis Center for Geotechnical Modeling (CGM) (Pires-Sturm and DeJong 2022, 2023). The 1m radius centrifuge was spun to 80g and a 40x viscosity pore fluid was used to address scaling effects (Garnier et al. 2007). Tests were conducted on the soils in Figure 6. Nine level-ground centrifuge models which consisted of a level ground profile within a flexible shear beam container with pore pressure and accelerometer sensor arrays were performed. Models were prepared via air pluviation to an initial relative density ($D_{R_initial}$) of about 40%. CPT profiling was collected throughout the tests to track relative density changes and $D_{probe}/D_{particle}$ effects. Models were repeatedly shaken at 1 Hz over 15 cycles of uniform sinusoidal acceleration at PBA = 0.1g – 0.2g to track liquefaction triggering and vertical strains, and to force densification to a final relative density ($D_{R,\,final}$) of about 90%.

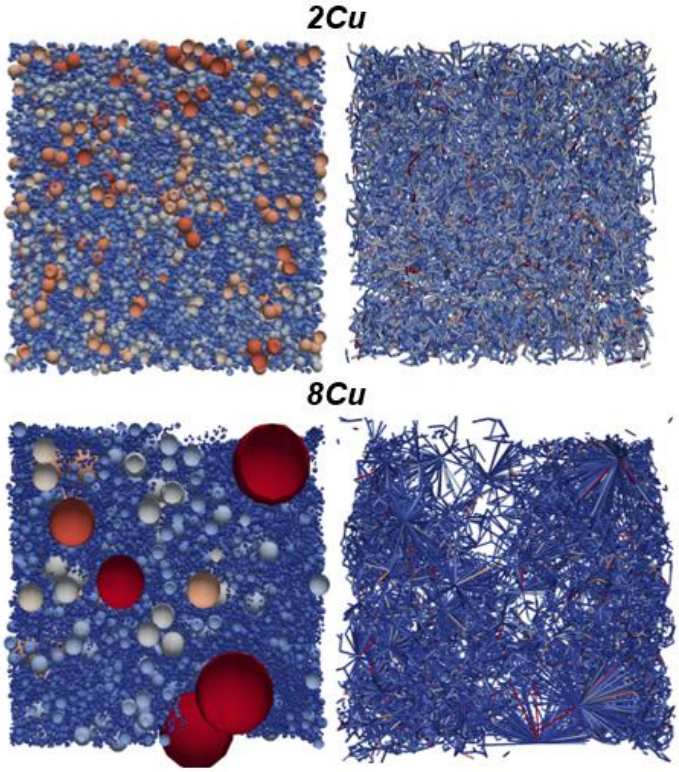


Figure 8. Assemblies and contact normal forces for 2Cu and 8Cu specimens for DEM simulations. Note: The particle's color is proportional to their size and the contact forces' color is proportional to their magnitude.

Representative results from the centrifuge tests are presented in Figure 10. The CPT penetration mechanism is compromised when the $D_{probe}/D_{particle}$ becomes too small. The presence of large particles, such that the probe to particle size ratio decreases by a factor of 10, results in measurements that are highly variable and elevated overall by a factor of about 2 relative to when the ratio is sufficiently high. As shown in the figure, increasing the probe size from 6 mm to 10 mm results in measurements with decreased variability and lower overall magnitude, though the

© ASCE

values are still elevated. Increasing C_u has an additional compounding effect, where a well graded soil with a smaller probe still has overall elevated measurements, which is consistent with the higher peak strength and stronger dilatancy observed in the laboratory tests, while the variability is decreased. The large particle effects can be mitigated further by increasing the probe size, such that a well graded soil with a larger probe has further reductions in variability.

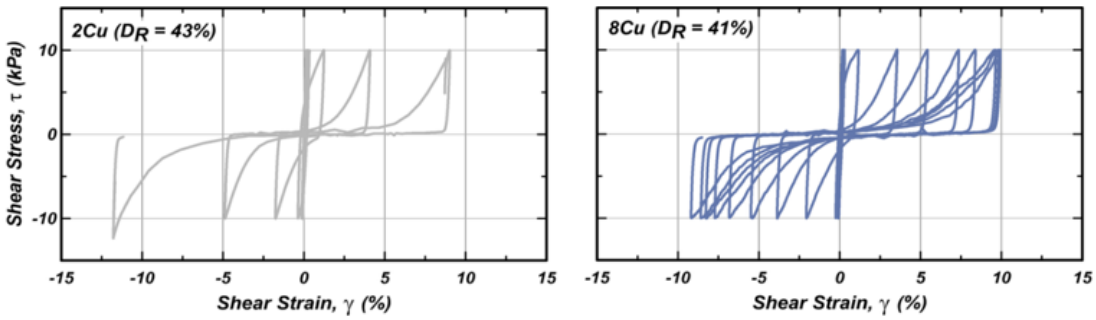


Figure 9. Effect of soil gradation (C_u) on undrained cyclic DSS response.

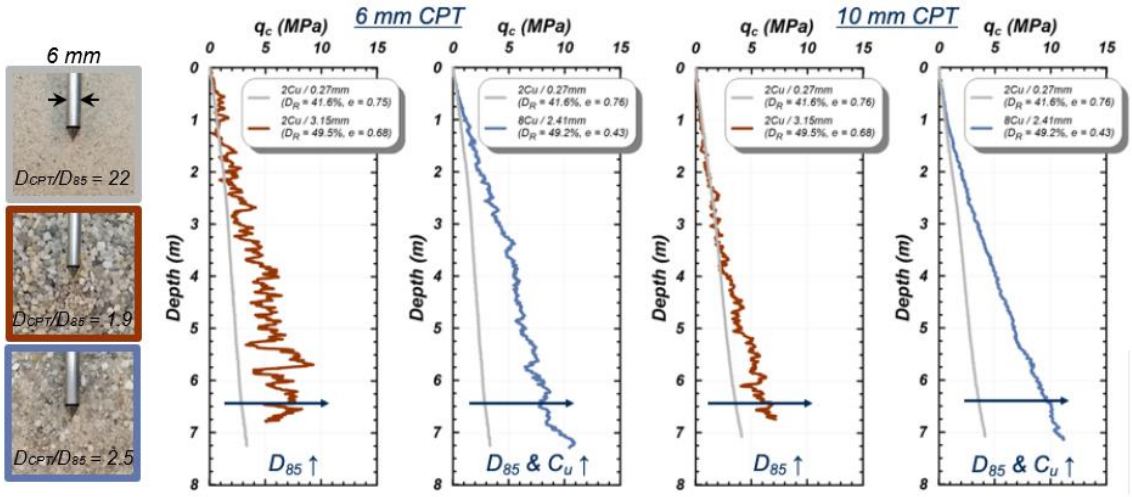


Figure 10. Effect of gradation and particle size on CPT q_c for different probe diameters. Adapted from Pires-Sturm and DeJong 2023).

Functions for calculating relative density in gravelly soil using Equation 1 were developed from the CPT data such as that presented in Figure 10. The C_P correction to address probe to particle size effects is developed based on poorly graded soils and under the assumptions that the effect is constant with confining stress, across the range of D_R, and can be formulated in combination with the C_P correction. The C_P correction shown in Figure 11a is:

$$C_P = 1.67e^{-0.55\left(\frac{D_{CPT}}{D_{85}}\right)} + 1 \quad (2)$$

© ASCE

For sufficiently large probe to particle ratios, the C_P correction term is essentially equal to 1 and thus not necessary because the particle size does not interfere with the probe measurements. As the probe to particle ratio decreases, the increasingly large particle sizes have an increasingly larger impact on the C_P correction term. When $D_{CPT}/D_{85} = 4$ (i.e., $D_{CPT} = 43.7$ mm, $D_{85} = 10.9$ mm) the q_t measurement is estimated to be elevated by about 20%. For $D_{CPT}/D_{85} < 2$, the correction is significant but becomes increasingly unreliable and its application should be exercised with caution.

The second term developed is to systematically account for changes in soil gradation (Figure 11b). The functional form of the C_{Cu} term is:

$$C_{Cu} = 1.0 + \frac{0.55}{1+(4/C_u)^{2.6}} \quad (3)$$

The C_{Cu} value increases from about 1 to 1.55 over a C_u range of 2 to 12, outside of which the C_{Cu} values are practically constant. This indicates that a poorly graded soil requires little to no coefficient of uniformity correction whereas a well graded soil requires a larger correction.

Together, $C_{total} = C_P C_{Cu}$, applies both Equation 2 and Equation 3 to demonstrate the combined effects of probe to particle size and soil gradation on the measurement adjustments necessary for well graded course grained soils (Figure 11c). The four stars in the figure represent different combinations of soil gradation (poorly graded vs. well graded) and particle size (sand vs. gravel, which thus affects $D_{probe}/D_{particle}$) when pushing a 15 cm^2 CPT, for example. $C_{total} = 1$ for a poorly graded sand while a $C_{total} \approx 2$ may be necessary for a well graded gravel. The C_{total} of about 2 is consistent with Skempton (1986) and Cubrinovski and Ishihara (1999) C_d ranges for SPTs. For poorly graded gravel and well graded sand the C_{total} values may be similar, but they are driven by the different effects of probe to particle size and gradation (the poorly graded gravel requires C_P correction while the well graded sand requires use of C_{Cu} to properly incorporate the effects of gradation).

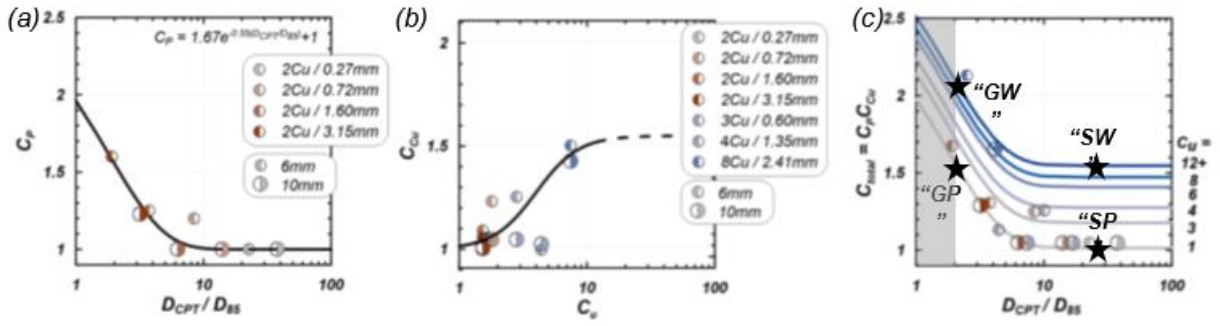


Figure 11. (a) Correction for probe to particle size effects using C_P, (b) incorporation of soil gradation (Cu) using C_{Cu}, and (c) combined total correction of $C_{total} = C_P C_{Cu}$.

Incorporating Equations 2 and 3 into Equation 1 and fitting to the CPT data produces the relative density correlations shown in Figure 12a where $\alpha = 0.7$, $\beta = 0.2$, and $\gamma = -1.12$, such that:

$$D_R = 0.7\left(\frac{q_{t1}}{P_a C_P C_{Cu}}\right)^{0.2} - 1.12 \quad (4)$$

© ASCE

Up to a 50% increase in CPT q_{t1} can occur as C_u increases (Figure 12b). For poorly graded soils, the correlation range of $C_u \approx 2$ to 6 indicates that C_u may significantly contribute to data scatter on which existing correlations are based (Figure 12c). The existing correlations from Jamiolkowski et al. (2001), Kulhawy and Mayne (1990), and Idriss and Boulanger (2008) follow a similar shift in the D_R correlation with q_{t1} as Equation 4.

Figure 13 shows the data from the centrifuge test results as the correction steps are applied from the generalized workflow for in situ characterization. As the initial direct profile measurements (q_c) are progressively corrected for stress normalization (q_{t1}) and adjusted for the effects of large particles (q_{t1}/C_p), ultimately the relative density estimates produced are more accurate, thus indicating reasonable robustness of the developed framework.

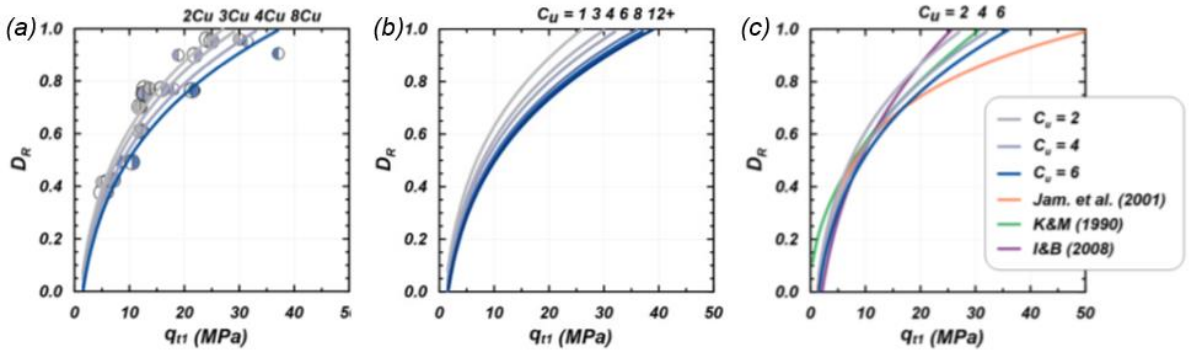


Figure 12. Relationship of q_{t1} with D_R (a) considering centrifuge data on synthetic soils, (b) across a C_u range from 1 to 12, and (c) compared to existing sand correlations.

LIQUEFACTION TRIGGERING

A suite of 150 shaking events with varying shaking intensity (I_a) and relative density were performed on the nine level-ground centrifuge models to assess the effect of soil gradation on liquefaction triggering (Pires-Sturm and DeJong 2022). The upper portion of each model had instrumentation arrays to capture soil responses, and CPT soundings were made to measure penetration resistance. Triggering was considered on a $r_u = 1$ basis. Figure 14 shows the spread of testing events where triggering occurred, with each soil type spanning the event space to allow for comparison of different soils with similar Arias intensity (I_a) and D_R values. The exceptions are the coarse, poorly graded gravels (shown in shades of red) which span the lower portion of the plot due to an inability to generate pore pressures and liquefy the soil, thereby limiting results to drained shake down events.

Using the shaking events on soils that were either well or poorly graded but with similar hydraulic conductivities, two event clusters in different regions of Figure 14 are compared to highlight the effects of D_R, I_a, and C_u on liquefaction triggering. Cluster 1 encompasses events with $D_R \approx 52\%$ and $I_a \approx 0.8$ m/s, whereas cluster 2 encompasses events with $D_R \approx 72\%$ and $I_a \approx 1.7$ m/s. For the soils which had lower relative density and lower shaking intensity (Cluster 1), a higher C_u resulted in a higher q_{t1} (e.g., $C_u = 8$ had $q_{t1} = 12$ MPa, $C_u = 2$ had $q_{t1} = 8$ MPa). However, the overall behavior was similar. The pore pressure (r_u) rises over the first few cycles and liquefaction occurs early on, therefore minimal cyclic resistance results in only small acceleration

© ASCE

propagating through the soil. For the higher C_u soil, r_u rises slightly slower and moderate cyclic resistance is generated at reversals, but the difference is not substantial.

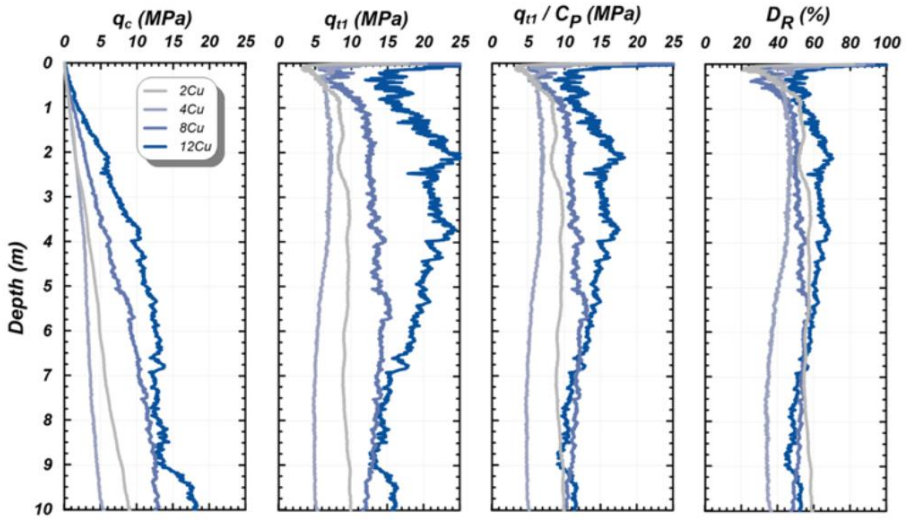


Figure 13. Example application of stress normalization, probe-to-particle size, and coefficient of uniformity factor to measured cone penetration resistance. (Note that 4Cu was prepared at D_R of about 40% while the other soils were prepared at ~60%).

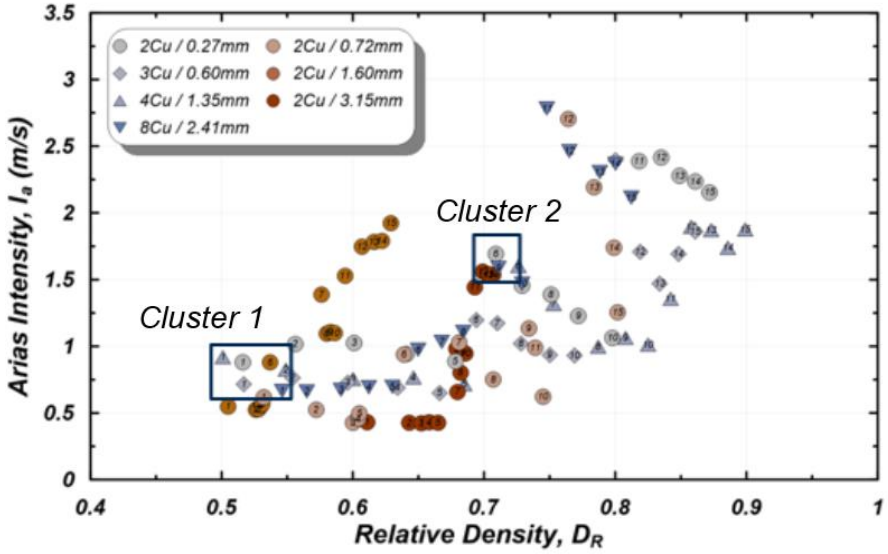


Figure 14. Centrifuge test combinations of D_R and shaking intensity (I_a) for range of soils tested. Inset box indicates test cluster shown in Figure 14

In contrast, the soil gradation had a larger effect on the soil response in the soils with higher relative density and greater shaking intensity (cluster 2), for which two representative shaking events with C_u = 2 and 8 are shown in Figure 15, respectively. As before, the higher C_u test has a larger q_{t1} measurement (i.e., 17 MPa compared with 13 MPa). In the poorly graded soil, the pore

© ASCE

pressure rises and persists within a few cycles, dilation spikes are observed, and cyclic shear resistance is mobilized, as evident in the stress-strain loops. Once again, the pore pressure rises slower in the well graded soil, but now strong oscillations are observed during loading due to the cyclic reversals and the strong dilative tendency for well graded soils. The increase in soil gradation also produces stronger peaks in the cyclic shear resistance shown in the stress-strain loops. These observations are consistent with the laboratory tests discussed earlier.

The effect of C_u on the liquefaction triggering curve for a $r_u = 1$ basis is presented in Figure 16. Overlaid for comparison is the Boulanger and Idriss (2015) triggering curve from the database for mostly clean, poorly graded sands with fines content < 5%, with a representative C_u assumed to be about 4 since the C_u is bounded by a practical lower limit of 2 in natural soils and a defined upper limit of 6 from the Unified Soil Classification System. An increase in soil gradation shifts the liquefaction triggering curve to the right because it increases the penetration resistance, an effect which is captured by the C_{Cu} factor. It is noted that the effect of probe to particle size, captured with C_P, is a measurement issue and does not contribute to the observed curve shifts. The triggering curves presented ranges for C_u values between 2 and 12 (due to how the C_{Cu} was formulated), representing up to a 50% increase in the penetration resistance depending on the soil gradation. This spread based on soil gradation may contribute to the uncertainty in the literature as to where the triggering curve exists. Note that probe to particle size effects do not influence this analysis and the cyclic resistance ratio is held constant because it has been shown to be relatively constant for different C_u values at the same D_R.

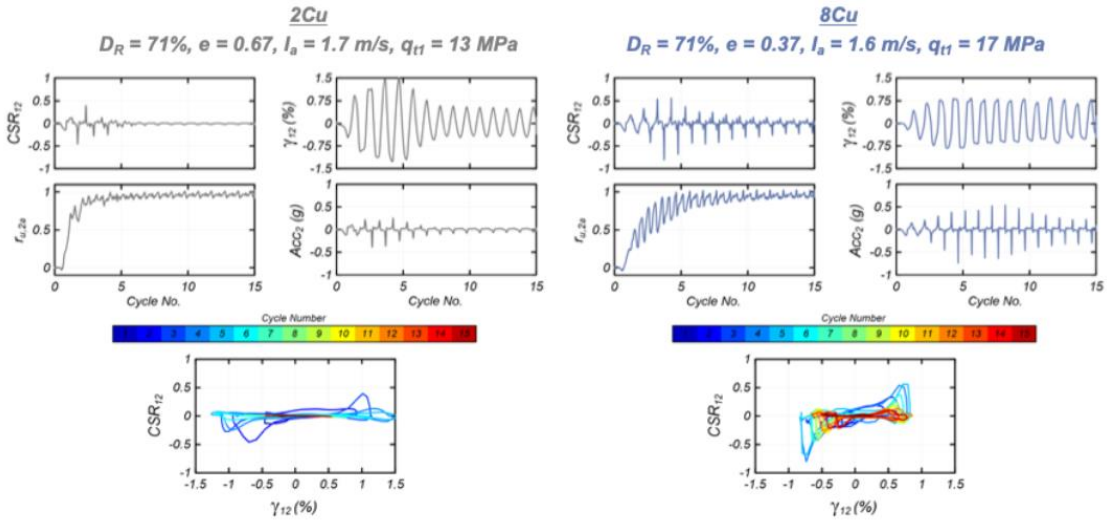


Figure 15. Response of pseudo-elements computed from within centrifuge tests for $2C_u$ and $8C_u$ soils at a D_R = 71% and subject to a shaking intensity of I_a = 1.6 m/s.

SHEAR AND VOLUMETRIC STRAINS

Centrifuge experiments were conducted to explore the influence of soil gradation on the system response (Carey et al. 2022 and 2023, Love 2022). Experiments were performed in the UC Davis CGM 9m radius centrifuge at 40g. Six models were tested, four with $D_{R,\,initial} \approx 40\%$ and two with $D_{R,\,initial} \approx 65\%$, with the slope profile specifications shown in Figure 17a. The models were

© ASCE

constructed in a container with transparent side walls which allowed tracking via colored markers and high-speed video. The models were subjected to repeated shaking events of increasing magnitude (1 Hz motion at PBAs of 0.13g–0.49g) with a ramp, hold, and decay range to respectively determine when triggering occurs, how strains accumulate, and when displacements arrest. Measurements were collected with a 10 mm CPT. Results are highlighted from the upslope and midslope regions in Figure 17a, revealing dynamic straining of all soil in which the poorly graded soils experience greater permanent displacements that are more non-uniform with depth as compared to the well graded soils (Figure 17b).

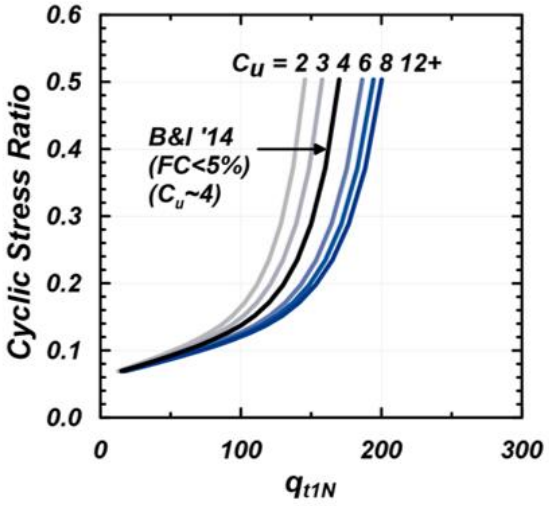


Figure 16. Mapping influence of C_u on Boulanger and Idriss (2015) liquefaction triggering curve assuming original curve represents a C_u of ~4.

Acceleration and pore pressure results are presented in Figure 18 for the upslope and midslope regions of a poorly graded (C_u = 2) and well graded (C_u = 12) soil. During shaking, all elements generate excess pore pressures (Δu) quickly, subsequently experiencing liquefaction triggering, and finally dissipating the Δu post-shaking. For the upslope measurements, the well graded soil generates more dilation (consistent with laboratory data) at stress reversals and dissipates the Δu about five times faster as compared to the poorly graded soil. For the midslope measurements, both the poorly and well graded soils experience much stronger dilation spikes relative to the upslope measurements. Additionally, the Δu in the midslope dissipates much faster in the well graded soil than in the poorly graded soil, similar to the observations of the upslope behavior in the two soil.

Pseudo element responses inside the models are color-coded by time in Figure 19, depicting the dynamic stress-strain responses and excess pore pressures generated during the shaking cycle (i.e., ramp, hold, and decay). Both upslope soils experience some dilation and therefore mobilize cyclic resistance during the stress reversals, though the effect is stronger in the well graded soil compared to the poorly graded soil. Similar dynamic responses are observed in the midslope measurements, but the evidence of static shear stress is more pronounced than in the upslope measurements. Both the 2 and 12 C_u soils in the midslope experience strong negative pore pressures, and strong dilation is mobilized during the stress reversals. The dynamic stress-strain

© ASCE

responses in the midslope are slightly more constrained for the well graded soil than the poorly graded soil.

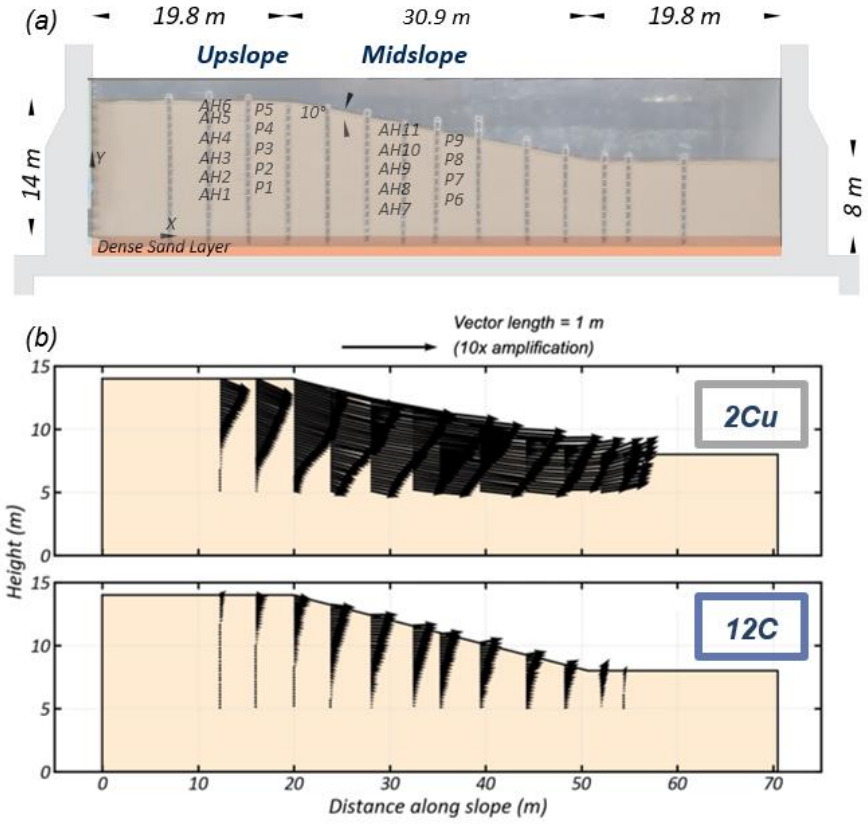


Figure 17. (a) Image/schematic of 9m centrifuge test in prototype scale indicating 'upslope' and 'midslope' regions presented in subsequent figures. (b) Final displacement vectors for C_u = 2 (upper) and C_u = 12 (lower) after shaking event with an I_a = 1.23 m/s. Adapted from Carey et al. 2022)

Excess pore pressure generation and dissipation at the upslope and midslope locations are further examined in Figure 20. For each test, the time duration above r_u = 0.5 during shaking was calculated from the Δu time series. As shown in Figure 20 for the upslope and midslope measurements, respectively, this elevated Δu time duration decreases by up to 80% as C_u increases from 2 to 12. As the hydraulic conductivities are comparable in all the models, this faster dissipation of excess pore water pressure in well graded soils is due to their lower initial void ratio and higher modulus.

Post-shaking, the permanent displacements and strains are quantified using measurements from the near-surface elements in the upslope and midslope regions (Figure 21). Displacements reduce significantly throughout the model as C_u increases from 2 to 12, with horizontal reductions between 50–80% and vertical reductions of more than 60%. In some cases, heaving of the ground surface is observed due to the soil dilation. Greater dilatancy is mobilized at the midslope due to the driving static shear stress. Over the same gradation range, shear strains reduce by 40–90% and the volumetric strains reduce by more than 60%, with dilation on the midslope.

© ASCE

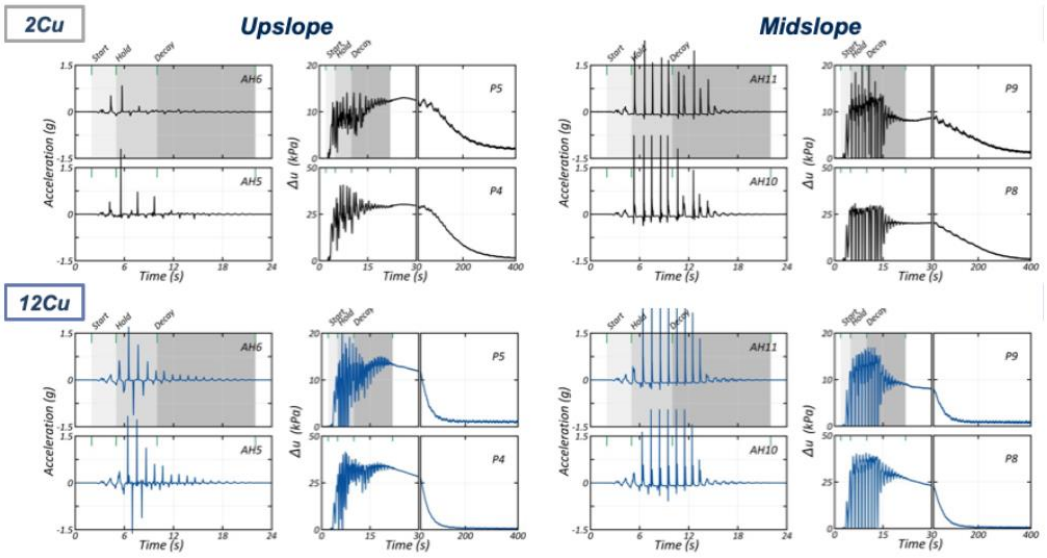


Figure 18. Acceleration and excess pore-pressure time histories of upslope and midslope sensors measured in 9m centrifuge tests of D_R = 45% sand with an I_a = 1.23 m/s.

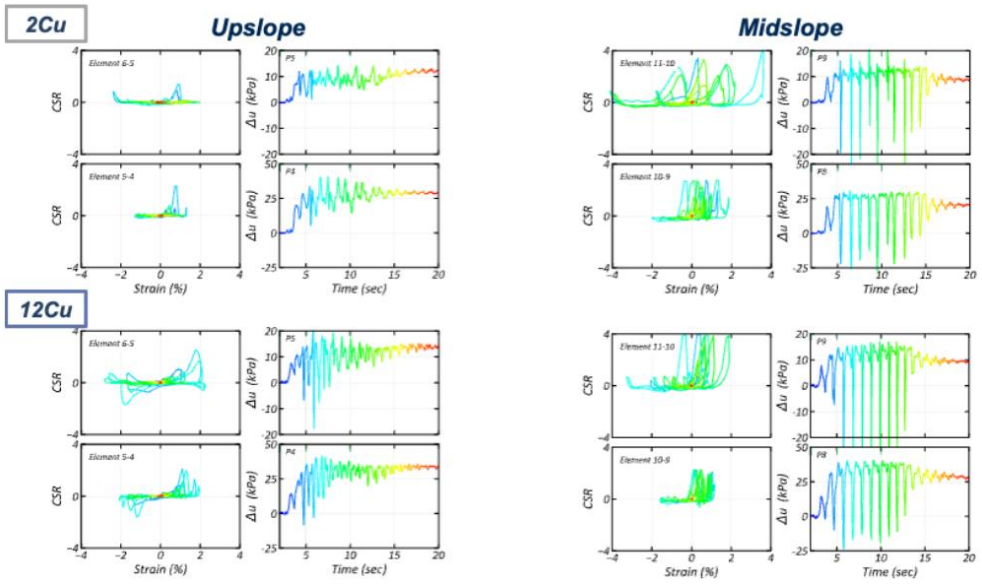


Figure 19. Stress-strain response of pseudo-elements and excess pore-pressure time histories in upslope and midslope in 9m centrifuge tests of D_R = 45% sand with an I_a = 1.23 m/s.

Temporal and spatial consideration of the strains reveals patterns in the model behaviors, with spatial distribution of shear strain shown in Figure 22 for the three phases of the shaking cycle (i.e., ramp, hold, decay). At both the upslope and midslope regions, strain accumulation begins once triggering occurs in the ramp phase and is followed by steady accumulation of strains that continues throughout the hold phase and into the decay phase, during which the strain accumulation slows and ultimately plateaus. The differences in the rate at which the strain

© ASCE

accumulation slows and stops in the decay phase is attributable to the differences in pore pressure dissipation for the models with the most extended accumulation occurring in the poorly graded model. The accumulated shear strain (γ) is about twice as large and more spatially localized in the poorly graded soil (C_u = 2) model as compared to the well graded soil (C_u = 12) model, with peak γ up to 10–12% for C_u = 2. Volumetric strain reveals that contraction occurs in the poorly graded soil whereas some dilation is observed in the well graded soil, particularly on the midslope.

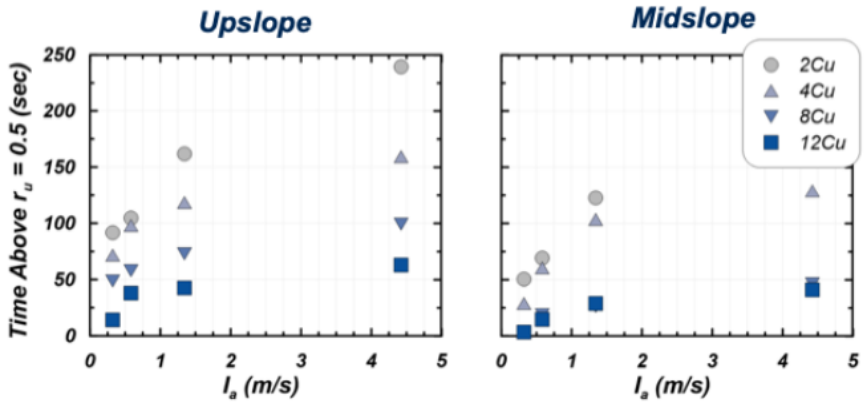


Figure 20. Time duration where excess pore pressure conditions remained above a r_u = 0.5 in the upslope and midslope as a function of I_a for a range of C_u conditions.

CONCLUSIONS

Characterizing and predicting the behavior of broadly graded gravelly soils for the design and analysis of civil infrastructure is a challenge. This paper has described a research program undertaken to help advance fundamental understanding and develop an approach for systematically considering the primary factors governing the problem and a process by which these factors could be incorporated in the engineering workflow. This research program used laboratory tests, numerical analyses, and physical models to gain insights into the fundamental changes that occur in the soil properties and behavior due to variations in particle size and gradation, address how the presence of large particles adversely influences characterization methods, and observe how these changes in properties may influence the system performance of slopes when subject to earthquake loading. This has enabled the following observations:

- The important characteristics and influence of well graded soils can best be captured considering the breadth of gradation, through C_u, and the size of the larger particles, through D_{85}. The percent gravel metric was found to be poorly defined and insufficient.
- The breadth of gradation is the primary factor that influences the changes in fundamental soil properties and behavior, including particle packing and void ratios (index properties), hydraulic conductivity (flow), stiffness and strength, stress-dilatancy, and critical state line (both slope and intercept). The magnitude of changes measured extend well beyond the typical range of values observed and expected for poorly graded soils. Examples include the void ratio for a given relative density decreasing by 50%, the dilation angle increasing by 6 degrees or more, the shear modulus increasing by 30%, and the slope of the critical state line decreasing by 50%.

© ASCE

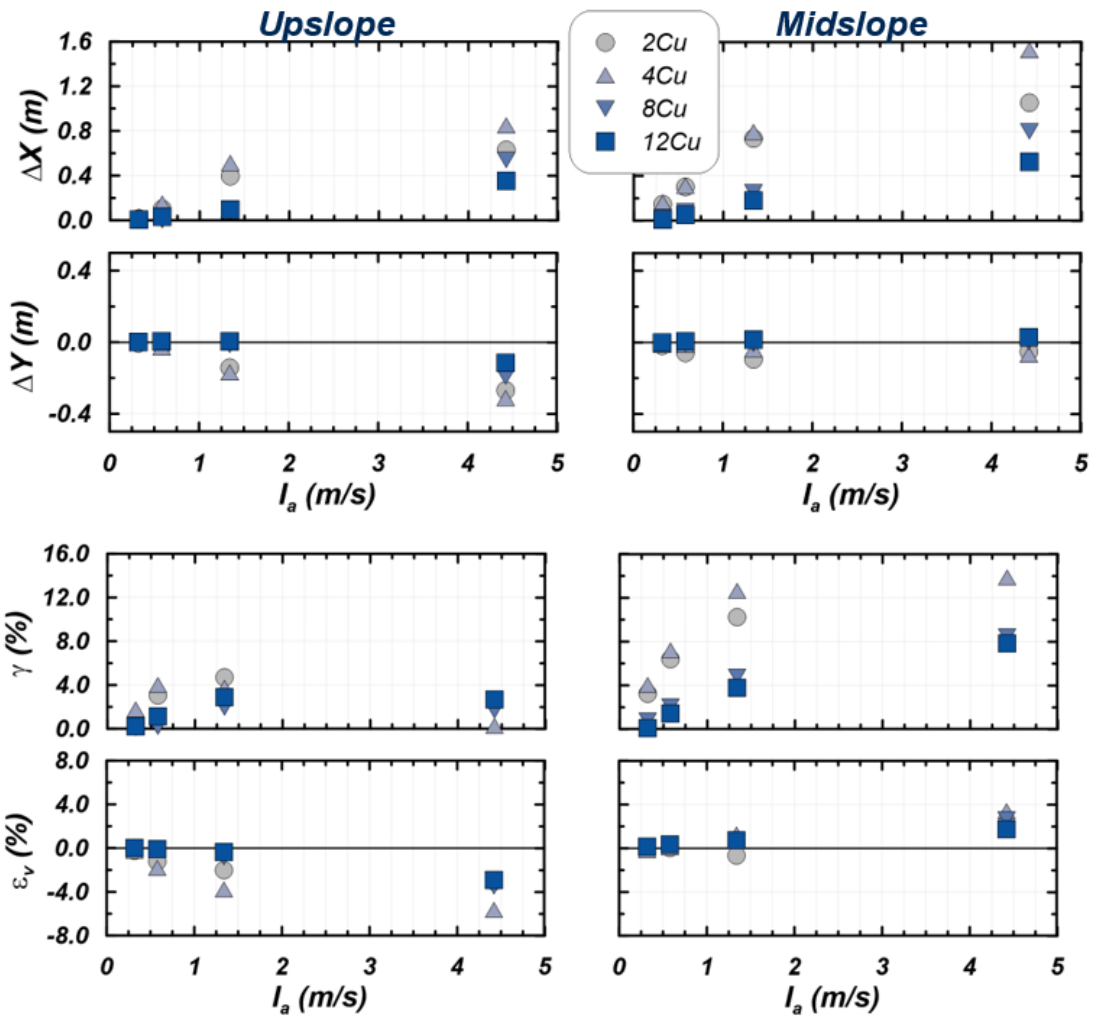


Figure 21. Total horizontal (ΔX) and vertical (ΔY) displacements as well as shear (γ) and volumetric (ε_v) strains for upslope and midslope as a function of I_a for a range of C_u conditions.

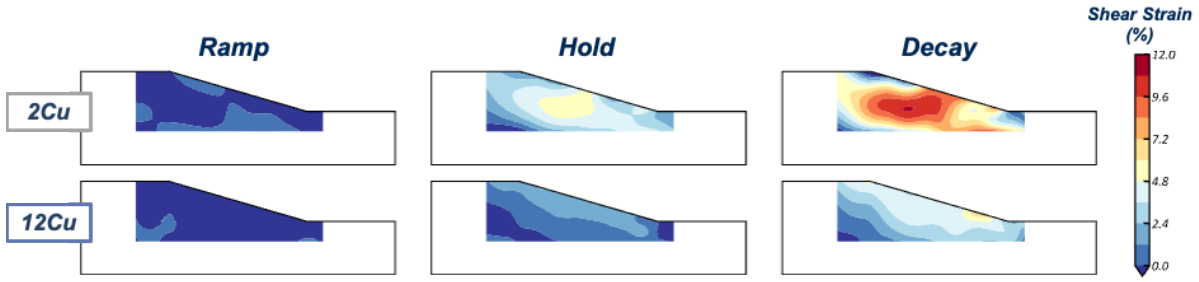


Figure 22. Spatial distribution of shear strain (γ) accumulation in 9m centrifuge tests of D_R =45% sand with an I_a = 1.23 m/s for Cu = 2 and 12 models for the ramp, hold, and decay segments of the shaking motion.

© ASCE

Table 1. Summary of applicability (✓ = applicable, X = not applicable, NN = not needed) of iBPT, SPT, and CPT to each soil type in the hypothetical example.

Zone	C_u	C_{Cu}	D_{85} (mm)	SPT	CPT	iBPT	C_P
Core	2.2	✓	2.1	✓	✓	✓	NN
Shell	50	✓	102	X	X	✓	✓
Alluvium	80	✓	30	X	X	✓	NN

- The presence of large particles directly influences the penetration resistance, producing artificially elevated values. The influence becomes significant when the D_{probe}/D_{85} ratio becomes less than about 4, at which point the measurement is elevated by about 20%. To correct for this influence, a C_P correction term (Equation 2) has been proposed to estimate a corrected value. The method produces a maximum correction of about 1.6 for D_{CPT}/D_{85} = 2; for ratios smaller than this, the correction exceeds the data set and should be used with caution.
- The influence of the breadth of gradation on penetration resistance directly influences the estimation of relative density based on cone penetration measurements. A C_{Cu} term (Equation 3) was proposed to explicitly incorporate the effect of gradation into the relative density calculation (and downstream analyses), where C_{Cu} = 1 for C_u = 2 and an increasingly larger correction up to a factor of 1.55 is applied as the soil becomes more well graded. The effect saturates for C_u > 12. The correction indicates that the q_{c1} for well graded soil at a given relative density may be up to 50% larger than a poorly graded soil at the same relative density. A comparison against previously developed D_R correlations suggests that the trends developed are reasonable and may partially explain the variations present between previously developed methods.
- Liquefaction triggering susceptibility was observed to be relatively insensitive to the breath of soil gradation. The lower void ratio and higher stiffness of well graded soils at the same relative density (and hydraulic conductivity) of poorly graded soils was observed to generate a r_u = 1 after a similar number of loading cycles, and in some cases reaching a r_u = 1 slightly earlier. These observations were consistent between laboratory and centrifuge modeling, as well as with prior studies.
- Propagating and combining the influence of soil gradation on cone tip resistance and liquefaction triggering susceptibility enabled reconsideration of the CPT-based liquefaction triggering curve. Increasing soil gradation produces a shift in the liquefaction triggering (r_u = 1 basis) curve to the right, with an increase of about 50% in q_{t1} across the C_u range of 2–12. The presence of large particles that artificially elevates the penetration resistance should be addressed prior to evaluating the triggering susceptibility.
- Centrifuge modeling using a submerged slope has provided insights into how soil gradation may influence the strains and displacements realized from earthquake shaking. In the tests performed the shear and volumetric strain accumulation was observed to decrease between 40–90% and become more spatially uniform with increasing gradation, with additional influences from relative density and shaking magnitude.

The potential implications of applying the results of this work on the representative idealized scenario presented in the Introduction are revisited here to exemplify how the insights generated

© ASCE

may be applicable to an industry project. The following observations can be made, as summarized in Table 1:

- The selection of a probe (e.g., SPT, CPT, iBPT) and relevant corrections must be carefully considered based on the soil properties.
- Applying the C_{Cu} correction to incorporate the influence of soil gradation would be appropriate for the soils present.
- For a poorly graded sand (e.g., the hypothetical dam core), any of the penetrometers could be used and no C_P correction is necessary. For a well graded gravel (e.g., the hypothetical dam shell), the SPT and CPT will not generate usable data and the iBPT will need the C_P correction applied due to the large gravel size. For a well graded sand (e.g., the hypothetical dam alluvium), the large C_P corrections required likely render the SPT and CPT unreasonable, but the iBPT could be used without the C_P correction.
- Implementation in practice will require the selection of representative values of C_u and D_{85} for stratigraphic units, perhaps using an approach similar to that employed in practice when using laboratory-based measurements of fines content. Note that this is primarily necessary for C_u between 2 and 12 as the C_{Cu} term saturates at higher values.
- Given that C_u was observed to have a greater effect on the penetration resistance, it is reasonable to expect the liquefaction triggering likelihood will remain largely unchanged.
- The strains and displacements realized by earthquake shaking may be lower than those estimated using soil properties and analysis methods based on the behavior and performance of systems constructed using poorly graded soils.

The results of this study document the importance of considering the breadth of soil gradation and particle size when performing characterization studies and estimating the engineering properties and behavior. It is intended that the insight provided herein will assist the geotechnical industry as they work to advance practice in this area. The applicability of these results to project sites must continue to be evaluated alongside complimentary work and existing approaches as continued advancement and refinement is needed.

ONLINE RESOURCES

A video of the 1st ASCE Prakash Lecture can be viewed at: https://www.youtube.com/watch?v=mFQ1bF8YWAM.

ACKNOWLEDGMENTS

The author would like to thank the UC Davis Center for Geotechnical Modeling, the National Science Foundation (NSF), the Natural Hazards Engineering Research Infrastructure (NHERI), the Pacific Earthquake Engineering Research (PEER) Center, and ConeTec for their contributions to this work. This work was supported in part by the National Science Foundation under grants CMMI-1300518 and CMMI-1916152, as well as by the NHERI shared use support of the UC Davis Center for Geotechnical Modeling under CMMI-1520581. Any opinions, findings, and conclusions or recommendations expressed in this material are those of the writer(s) and do not necessarily reflect the views of the National Science Foundation. The support and contributions of Sharif Ahmed, Mandeep Basson, Anna Chiaradonna, Francisco Humire, Kevin Kuei, Nathan Love, Alex Pires-Sturm, and Rachel Reardon are particularly appreciated.

© ASCE

REFERENCES

Ahmed, S. S., A. Martinez, and J. T. DeJong. (2023). "Effect of Gradation on the Strength and Stress-Dilation Behavior of Coarse-Grained Soils in Drained and Undrained Triaxial Compression." ASCE *JGGE*. 149(5):04023019.

Basson, M. S., A. Martinez, and J. T. DeJong. (2024). "DEM Investigation of the Effect of Gradation on the Strenght, Dilatancy, and Fabric Evolution of Coarse-Grained Soils." ASCE *JGGE*. 150(8):04024060.

Been, K., and M. G. Jefferies. (1985). "A state parameter for sands." *Géotechnique*. 35(2): 99–112.

Bolton, M. D. (1986). "The strength and dilatancy of sands." *Géotechnique*. 36(1): 65–78.

Bolton, M. D., M. W. Gui, J. Garnier, J. F. Corte, G. Bagge, J. Laue, and R. Renzi. (1999). "Centrifuge cone penetration tests in sand." *Géotechnique*. 49(4):543–552.

Boulanger, R. W., and I. M. Idriss. (2015). "CPT-based liquefaction triggering procedure." ASCE *JGGE*. 142(2): 04015065.

BS 5930:2020. (2020). *Code of practice for ground investigations* (British Standard).

Carey, T. J., A. Chiaradonna, N. C. Love, D. W. Wilson, K. Ziotopoulou, A. Martinez, and J. T. DeJong. (2022). "Effect of soil gradation on embankment response during liquefaction: A centrifuge testing program." *SDEE*. 157:107221.

Carey, T. J., N. C. Love, and J. T. DeJong. (2023). "The Liquefction and Cyclic Mobility Performance of Embankment Systems Constructed with Different Sand Gradations." ASCE *JGGE*. 149(10):04023084.

Cubrinovski, M., and K. Ishihara. (1999). "Empirical correlation between SPT N-value and relative density for sandy soils." *Soils & Foundations*. 39 (5): 61–71.

DeJong, J. T., M. Ghafghazi, A. P. Sturm, D. W. Wilson, J. den Dulk, R. J. Armstrong, A. Perez, and C. A. Davis. (2017). "Instrumented Becker penetration test I: Equipment, operation, and performance." ASCE *JGGE*. 143(9):04017062.

Garnier, J., C. Gaudin, S. M. Springman, P. J. Culligan, D. Goodings, D. Konig, B. Kutter, R. Phillips, M. F. Randolph, and L. Thorel. (2007). "Catalogue of scaling laws and similitude questions in geotechnical centrifuge modelling." *Int. J. Phys. Model. Geotech.* 7(3):1–23.

Ghafghazi, M., and J. T. DeJong. (2016). "A review of liquefaction case histories in gravelly soils using SPT based triggering curves." *69th Canadian Geotechnical Conf.*, London: International Society for Soil Mechanics and Geotechnical Engineering.

Ghafghazi, M., J. T. DeJong, A. P. Sturm, and C. E. Temple. (2017). "Instrumented Becker penetration test II: iBPT-SPT correlation for characterization and liquefaction assessment of gravelly soils." ASCE *JGGE*. 143(9):04017063.

Hazen, A. (1911). "Discussion of 'Dams on Sand Foundations,' by A.C.Koenig." *ASCE Transactions*. 73: 193-203.

Humire, F. A. (2022). *Liquefaction and post-liquefaction behavior of coarse-grained soils*. Ph.D. dissertation, Dept. of Civil and Environmental Engineering, Univ. of California, Davis.

Idriss, I. M., and R. W. Boulanger. (2008). *Soil liquefaction during earthquakes*. Oakland, CA: Earthquake Engineering Research Institute.

Iqbal, M. S. (2004). *Discrete element modeling of cone penetration testing in coarse grain soils*. M.S. thesis, Dept. of Civil and Environmental Engineering, Univ. of Alberta.

© ASCE

Jamiolkowski, M., D. Presti, and M. Manassero. (2001). “Evaluation of relative density and shear strength of sands from CPT and DMT.” *Soil Behav. Soft Ground Constr.* 7(119):201–238.

Kuei, K. C., J. T. DeJong, and A. Martinez. (2020). “Particle Size Effects on the Strength and Fabrice of Granular Media.” *ASCE Geo-Congress 2020: Modeling, Geomaterials, and Site Characterization* (GSP 317),.

Kulhawy, F. H., and P. W. Mayne. (1990). Manual on estimating soil properties for foundation design. EPRI EL-6800. Electric Power Research Institute. Palo Alto, CA.

Love, N. (2022). *The Effect of Sand Gradation on the Dynamic Performance of Embankments*. M.S.C.E. thesis, University of California, Davis.

Pires-Sturm, A., and A. Lutz. (2023). “Regulatory Perspective on Penetration Testing in Gravelly Soils.” *ASDSO Dam Safety Conference*, Palm Springs, CA, September 18-22, 2022.

Pires-Sturm, A., R. Jaeger, and J. T. DeJong. (2022). “Estimating Maximum and Minimum Void Ratio from Index Parameters.” *ASDSO Dam Safety Conference*, Baltimore, MD, September 12-22, 2023.

Pires-Sturm, A. P., and J. T. DeJong. (2022). “Influence of particle size and gradation on liquefaction potential and dynamic response.” ASCE *JGGE*. 148(6):04022045.

Pires-Sturm, A. P., and J. T. DeJong. (2023). “Cone Penetration Resistance in Coarse-Grained Gravelly Soils.” ASCE *JGGE*. 149(1):04022120.

Reardon, R. A. (2021). *Monotonic and Cyclic Direct Simple Shear Testing of Coarse-Grained Soils*. M.S.C.E. thesis, Dept. of Civil and Environmental Engineering, Univ. of California, Davis.

Skempton, A. W. (1986). “Standard penetration test procedures and the effects in sands of overburden pressure, relative density, particle size, ageing and overconsolidation.” *Geotechnique*. 36(3):425-447.

Sturm, A. P. (2019). *On the liquefaction potential of gravelly soils: Characterization, triggering and performance*. Ph.D. dissertation, Dept. of Civil and Environmental Engineering, Univ. of California Davis.

© ASCE

Development of a Modified Cam-Clay Model for Unsaturated Soils under Elevated Temperatures

Toan Duc Cao, Ph.D., M.ASCE[1]

[1]Research Assistant Professor, Dept. of Civil Engineering Technology, Environmental Management, and Safety, Rochester Institute of Technology, New York, NY.
Email: tdcite@rit.edu

ABSTRACT

Understanding the temperature dependency of the mechanical behavior of unsaturated soils is crucial for modeling their performance in environments subject to significant thermal variations. This study addresses the need for advanced constitutive models to support emerging applications in geotechnical and geoenvironmental engineering. A modified Cam-Clay model was developed to incorporate nonisothermal formulations for soil-suction stress, effective stress, and the water retention curve, enabling the prediction of thermo-elastoplastic behavior in unsaturated soils. The formulation accounts for temperature effects on key parameters, including enthalpy, contact angle, and surface tension. A series of closed-form equations is introduced to describe temperature-dependent suction and yield mechanisms within a critical state framework. The model is calibrated and validated using experimental datasets, including suction-controlled triaxial tests and volumetric strain measurements at elevated temperatures. Results show strong agreement with observed data and improved accuracy compared to existing models. The proposed framework offers a robust and predictive tool for analyzing temperature-sensitive behavior in unsaturated soils, with applications in nuclear waste containment, energy geostructures, and climate-resilient infrastructure.

INTRODUCTION

The mechanical behavior of unsaturated soils under coupled thermal, hydraulic, and mechanical (THM) loading conditions is of growing importance in modern geotechnical engineering. Applications such as nuclear waste disposal facilities, energy geostructures, geothermal systems, and underground thermal energy storage frequently expose geomaterials to elevated temperatures while they remain in unsaturated states. These complex environments necessitate constitutive models that can accurately simulate the interactions among temperature, suction, and stress responses.

In geotechnical engineering, modeling the stress-strain behavior of unsaturated soils under thermal influences has received increasing attention, particularly in the context of energy systems, climate-sensitive infrastructure, and nuclear waste containment (McCartney et al. 2019). A major step toward realistic simulation of natural slopes and engineered embankments under elevated temperatures is the development of constitutive equations that incorporate the influence of temperature on water retention, shear strength, and deformation behavior.

Experimental studies have consistently identified several key thermal effects on unsaturated soils:

© ASCE

- Elevated temperatures reduce air-entry suction and shift the soil-water retention curve (SWRC) downward, especially in silts and clays (e.g., Bachmann et al. 2002; Vahedifard et al. 2018).
- Both elastic and plastic compressibility components increase with temperature (Romero et al. 2001; Tang and Cui 2011).
- Yield surfaces shrink at constant suction as temperature rises (Tang et al. 2008; Ye et al. 2012).
- Critical state friction angle remains largely unaffected by temperature (Cekerevac and Laloui 2004; Mašín and Khalili 2012).
- Higher temperatures enhance creep deformation due to reduced viscosity (Fox and Edil 2011).
- Shear modulus and tensile strength of fine-grained soils decrease under heating (Cao et al. 2021; Salimi et al. 2021).
- Unsaturated soils undergo temperature-induced volumetric changes, depending on stress history and plasticity (Cui et al. 2011; Hueckel and Baldi 1990).

Several thermo-mechanical constitutive models have been proposed for unsaturated soils (Bolzon and Schrefler 2005; François and Laloui 2008; Mašín and Khalili 2012), most of which extend isothermal frameworks, such as the Modified Cam-Clay model, by incorporating thermal dependencies via Bishop's effective stress principle (Bishop 1959). These models typically attribute thermal effects to changes in surface tension, which influence suction and the degree of saturation. However, growing evidence suggests that this simplification may be insufficient for fine-grained soils. Experimental findings indicate that temperature also affects enthalpy, contact angle, and soil microstructure, which influence effective stress and SWRC beyond surface tension alone (Grant and Salehzadeh 1996; Vahedifard et al. 2018, 2019).

Recent developments have broadened the modeling framework by considering plasticity mechanisms, overconsolidation effects, bounding surface formulations, and temperature-dependent hysteresis. For example, François and Laloui (2008) employed a unified approach combining elastoplasticity and multi-mechanism plasticity. Zhou et al. (2012a; b) incorporated cyclic thermal effects within a bounding surface context, while others (e.g., Coccia and McCartney 2016) highlighted thermally enhanced creep in overconsolidated clays.

Despite these advances, current models often inadequately capture temperature-induced changes in effective stress and volumetric behavior, particularly when assuming that surface tension alone governs thermal dependence. A more physically accurate approach requires accounting for the combined effects of temperature on surface tension, contact angle, and suction stress, which directly affect the constitutive response of unsaturated soils.

This study presents a thermomechanically coupled extension of the Modified Cam-Clay model for unsaturated soils, integrating temperature-dependent formulations for suction stress, yield behavior, and hardening mechanisms within a critical state framework. The model builds upon a generalized effective stress principle and introduces closed-form expressions for nonisothermal water retention and suction stress behavior. Validation is conducted against experimental data from suction-controlled triaxial and isotropic compression tests at elevated temperatures. The proposed model provides a robust and unified framework for simulating unsaturated soil behavior under realistic THM conditions and holds significant promise for the analysis and design of geotechnical systems subjected to thermal loading.

© ASCE

FORMULATION DEVELOPMENT

Soil water retention model

Lu (2016) proposed a soil-water retention curve (SWRC) model that is applicable across the full range of matric suction, encompassing both the capillary and adsorption regions. Expanding upon the widely used van Genuchten (1980) model, Lu's formulation expresses the SWRC in terms of the effective degree of saturation, S_e, as follows:

$$S_e = 0.5\left[1 - erf\left(\sqrt{2}\frac{\psi - \psi_c}{\psi_c}\right)\right][1 + (\alpha\psi)^n]^{1/n-1} \tag{1}$$

where $erf()$ denotes the error function, ψ_c is the cavitation suction, ψ represents the matric suction, α is a fitting parameter inversely related to the air-entry suction (with units of 1/kPa), and n is the pore-size distribution fitting parameter.

Closed-form solutions for suction stress and effective stress at elevated temperatures

Bishop's effective stress formulation can be reformulated by interpreting the term $-\chi(u_a - u_w)$ as suction stress, following the approach proposed by Lu and Likos (2006), as:

$$\sigma' = (\sigma - u_a) - \sigma^s \tag{2}$$

where σ' is the effective stress, σ is the total stress, u_a is the pore air pressure (assumed to be equal to atmospheric pressure), and σ^s is the suction stress.

The suction stress under elevated temperatures is presented in Cao et al. (2021) as:

$$\sigma^s = -S_e\psi\left(\frac{\beta_{T_r} + T_r}{\beta + T}\right) \tag{3}$$

where β and β_{T_r} are regression parameters, defined in terms of contact angle, surface tension, and enthalpy of immersion.

Depending on the availability of fitting parameters, any of the extended SWRC models proposed by Vahedifard et al. (2018) can be employed to define S_e in Eq. (4). The temperature-dependent formulation of Lu's model can then be incorporated into Eqs. (4) and (2) to derive a complete expression for temperature-dependent effective stress. The resulting equations for suction stress and effective stress at varying temperatures are given as follows:

$$\sigma^s = -0.5\left[1 - erf\left(\sqrt{2}\frac{\psi\left(\frac{\beta_{T_r} + T_r}{\beta + T}\right) - \psi_c}{\psi_c}\right)\right]\left[1 + \left(\alpha\psi\left(\frac{\beta_{T_r} + T_r}{\beta + T}\right)\right)^n\right]^{1/n-1}\psi\left(\frac{\beta_{T_r} + T_r}{\beta + T}\right) \tag{4}$$

© ASCE

$$\sigma' = \left(\sigma - u_a\right) + 0.5\left[1 - erf\left(\sqrt{2}\frac{\psi\left(\frac{\beta_{T_r} + T_r}{\beta + T}\right) - \psi_c}{\psi_c}\right)\right]\left[1 + \left(\alpha\psi\left(\frac{\beta_{T_r} + T_r}{\beta + T}\right)\right)^n\right]^{1/n-1}\psi\left(\frac{\beta_{T_r} + T_r}{\beta + T}\right) \quad (5)$$

Closed-form solutions for the Modified Cam-Clay Model

The volumetric strain is decomposed into three components:

$$d\varepsilon = d\varepsilon_e + d\varepsilon_T + d\varepsilon_p \quad (6)$$

where $d\varepsilon_T$, $d\varepsilon_e$ and $d\varepsilon_p$ are the thermal elastic strain, the elastic strain, and the plastic strain, and $d\varepsilon$ is the total strain.

Temperature-induced elastic strain is written in Cekerevac and Laloui (2004):

$$d\varepsilon_T = -3\alpha_e dT \quad (7)$$

The elastic and plastic strains under elevated temperature are rewritten (Cao and Sun 2025):

$$d\varepsilon_e = \frac{\kappa}{v_0}\left[1 + B\ln\left(\frac{T}{T_r}\right)\right]\frac{d\sigma'}{\sigma'} \quad (8)$$

$$d\varepsilon_p = \frac{1}{\left(H_0 + h_T\Delta T\right)\left[1 + a\psi\left(\frac{\beta_{T_r} + T_r}{\beta + T}\right)\right]}\frac{d\sigma'}{\sigma'} \quad (9)$$

where α_e is the isotropic thermal expansion coefficient of the solid skeleton, $h_T = 1.67\times10^{-4}K^{-1}$ has been assumed by Romero et al. (2015), H_0 is the hardening modulus for isotropic compression at full saturation (or plastic modulus during isotropic compression), a is a parameter that depends on material characteristics; κ is the slopes of virgin elastic unloading line.

The decrease in yield stress with increasing temperature, as proposed by Hueckel and Borsetto (1990) in the context of thermal consolidation and variations in pre-consolidation pressure, can be represented by the following expression (Sultan et al. 2002):

$$\sigma'_{cT} = \sigma'_{c0}e^{-3\alpha^p\Delta T\left(H_0 + h_T\Delta T\right)} \quad (10)$$

where the positive scalar function α^p has the units of a thermal dilatation coefficient, so that the term of $3\alpha^p\Delta T$ represents the equivalent unrecoverable volumetric strain. σ'_{c0} is a reference stress given by:

© ASCE

$$\sigma'_{c0} = \sigma'_0 e^{H_0 \varepsilon_p} \tag{11}$$

where σ'_0 is the initial elastic limit at the reference temperature?

Accordingly, the yield stress under nonisothermal conditions is described in terms of thermal and matric suction evolutions as:

$$\sigma'_{c\psi T}(\psi, T) = \sigma'_c \left(\frac{\sigma'_{cT}}{\sigma'_c} \right)^{1+a\psi\left(\frac{\beta_{T_r}+T_r}{\beta+T}\right)} \tag{12}$$

Replacing Eqs. 10 and 11 into Eq. 12, the complete form of the yield stress for the proposed thermo-elastoplastic model of unsaturated soils for isotropic conditions becomes:

$$\sigma'_{c\psi T}(\psi, T) = \sigma'_c \left(\frac{\sigma'_0}{\sigma'_c} \right)^{1+a\psi\left(\frac{\beta_{T_r}+T_r}{\beta+T}\right)} e^{\left(\varepsilon_p - 3\alpha^p \Delta T\right)\left[1+a\psi\left(\frac{\beta_{T_r}+T_r}{\beta+T}\right)\right](H_0 + h_T \Delta T)} \tag{13}$$

Here's the extended modified Cam-Clay (MCC) yield function for unsaturated soils under thermo-mechanical loading, incorporating suction and temperature effects:

$$f(\sigma', q, \psi, T) = q^2 - M^2 \left(\sigma' + \sigma_s\right)\left(\sigma' - \sigma'_{c\psi T}\right) = 0 \tag{14}$$

where q is the deviatoric stress, and M is the slope of the Critical State Line (CSL) as a function of the angle of friction at critical state:

$$M = \frac{6\sin\phi'}{3 - \sin\phi'} \tag{15}$$

where ϕ' is the critical state friction angle of the soil. The majority of past studies indicate that the critical state friction angle remains unaffected by temperature (Mašín and Khalili 2012; Yavari et al. 2016).

VALIDATION AGAINST EXPERIMENTAL DATA

Suction stress

The predicted temperature-dependent suction stress values obtained from the proposed formulations are compared with experimental results reported by Ye et al. (2012) for Gaomiaozi bentonite (GMZ01). The parameters used in the prediction are as follows: $\Delta h_{(T_r)}$ = -0.516 J/m2, T_r = 293K, n = 1.31, α = 0.079 kPa-1 and ψ_c = 550 kPa.

Figures 1a and 1b compare the suction stress values predicted by the proposed model (Eq. 4) with the experimental results reported by Ye et al. (2012) for GMZ01 bentonite at temperatures of 20 °C and 60 °C, respectively. The comparison reveals strong agreement between the model

© ASCE

predictions and measured data. In both cases, suction stress is calculated using the widely adopted relationship that defines it as the product of matric suction and the effective degree of saturation-a formulation that has been extensively validated under ambient conditions (e.g., Lu et al. 2010). Nevertheless, the applicability of this assumption under elevated temperature conditions remains uncertain. Future studies should prioritize obtaining temperature-controlled triaxial test data, which would enable direct back-calculation of suction stress. Such data are essential for thoroughly evaluating the proposed model and comparing it with alternative suction stress formulations under thermal effects.

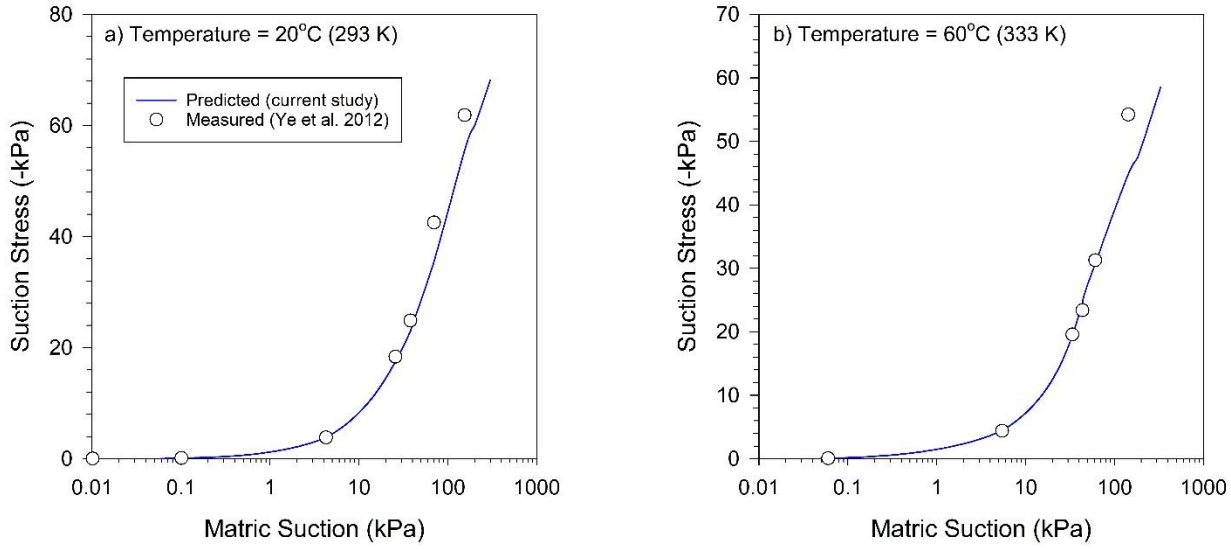


Figure 1. Measured and predicted suction stress for GMZ01 bentonite at temperatures 20ºC and 60ºC

Stress-Strain Relationship and Volume Change for Suction-Controlled Triaxial Compression.

The predictive performance of the proposed thermo-hydro-mechanical constitutive model was assessed through comparison with experimental results from suction-controlled triaxial compression tests on Bourke silt, conducted by Uchaipichat and Khalili (2009). The evaluation includes both deviatoric stress-axial strain and volumetric strain-axial strain responses under various temperatures and matric suction conditions. The model input parameters used in the analysis are summarized as, $\Delta h_{(T_r)}$ = -0.516 J/m2, T_r = 293K, n = 1.54, α = 0.0206 kPa-1, ψ_c = 550 kPa, κ = 0.006, B = 0.825, h_T = 1.67x10-4 K^{-1}, a = 0.0015, α_e = 10-5 K-1, α^p = 10-4 K^{-1}, λ_0 =0.09, and e_0 =0.63.

Figure 2 presents the comparison between predicted and measured deviatoric stress-axial strain responses for Bourke silt under an initial net mean stress of 100 kPa and a matric suction of 100 kPa. The proposed model effectively captures the overall trends and magnitudes of the experimental data across varying temperatures, demonstrating its capability to simulate the stress-strain behavior of unsaturated soils under thermal loading conditions. Notably, the model's predictions align more closely with the experimental results than those of Xiong et al. (2016), highlighting improved accuracy and robustness.

© ASCE

Similarly, Figure 3 compares the predicted and observed volumetric strain-axial strain responses under identical loading and suction conditions. The model accurately reproduces the thermal influence on soil compressibility and contraction, further validating its reliability. Across the full range of temperatures tested, the current model consistently provides a better fit to experimental trends than previously published models.

This strong agreement between numerical predictions and laboratory data confirms the effectiveness of the proposed framework in capturing the coupled thermal-hydro-mechanical behavior of unsaturated soils. The results affirm the model's predictive capacity for temperature-dependent stress-strain and volumetric responses, underscoring its potential application in both research and engineering practice.

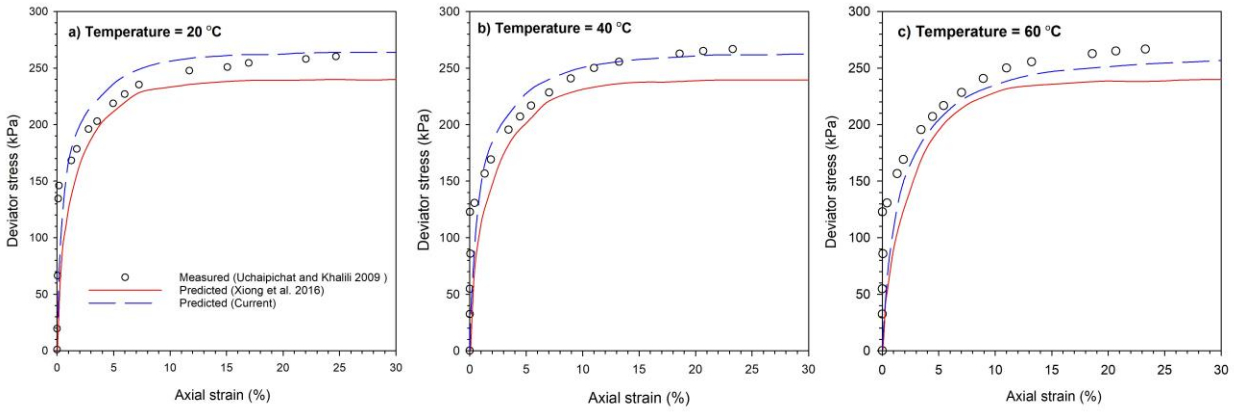


Figure 2. Deviatoric Stress-Axial Strain Relationships for Bourke Silt at Elevated Temperatures

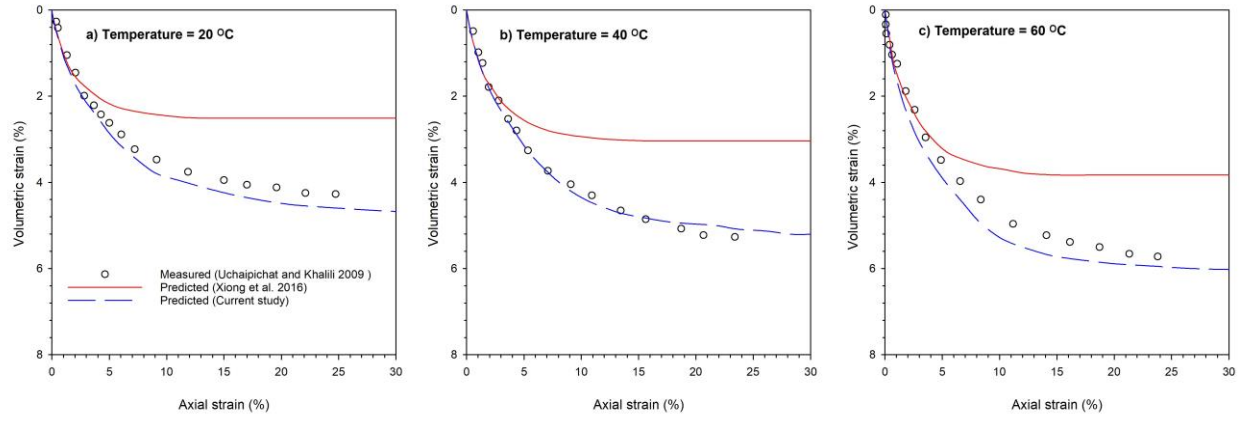


Figure 3. Volumetric Strain-Axial Strain Relationships for Bourke Silt at Elevated Temperatures

CONCLUSIONS

This study presents a thermomechanically coupled extension of the Modified Cam-Clay model tailored for unsaturated soils under elevated temperatures. By incorporating temperature-

© ASCE

dependent formulations for suction stress and water retention behavior into the critical state framework, the model enhances our ability to predict soil responses under realistic environmental conditions.

Key findings include:

- A closed-form formulation for suction stress that incorporates temperature effects via changes in surface tension, contact angle, and enthalpy of immersion.
- An extended SWRC and effective stress model that provides a more physically representative foundation for nonisothermal behavior.
- Thermally influenced yield surface evolution and hardening modulus are embedded into the Cam-Clay framework, enabling the prediction of thermal softening, contraction, and collapse.
- The proposed model demonstrates strong agreement with experimental data for both suction stress and stress-strain behavior, outperforming previous models in capturing temperature-dependent soil mechanics.

Overall, the model provides a robust and unified constitutive framework suitable for simulating the thermo-hydro-mechanical behavior of unsaturated soils. Its application spans geotechnical systems subjected to high temperature conditions, such as nuclear waste repositories, energy geostructures, and underground thermal storage systems. Future work will focus on extending the model to accommodate anisotropy, rate dependency, and broader validation across soil types and field scenarios.

ACKNOWLEDGEMENT

This research was supported in part by the U.S. Nuclear Regulatory Commission under Grant No. 31310022M0034. The author gratefully acknowledges this support. Any opinions, findings, and conclusions or recommendations expressed in this paper are those of the author and do not necessarily reflect the views of the U.S. Nuclear Regulatory Commission.

REFERENCES

Bachmann, J., R. Horton, S. A. Grant, and R. R. van der Ploeg. 2002. “Temperature Dependence of Water Retention Curves for Wettable and Water-Repellent Soils.” *Soil Science Society of America Journal*, 66 (1): 44–52.

Bishop, A. W. 1959. “The Principle of Effective Stress.” *Teknisk Ukeblad*, 39: 859–863.

Bolzon, G., and B. A. Schrefler. 2005. “Thermal effects in partially saturated soils: a constitutive model.” *Int J Numer Anal Methods Geomech*, 29 (9): 861–877. John Wiley & Sons, Ltd.

Cao, T. D., and L. Sun. 2025. “Temperature-dependent elastoplastic behavior of low plasticity unsaturated soils.” *Acta Geotech*, 20, 2889–2909.

Cao, T. D., S. K. Thota, F. Vahedifard, and A. Amirlatifi. 2021. “General Thermal Conductivity Function for Unsaturated Soils Considering Effects of Water Content, Temperature, and Confining Pressure.” *Journal of Geotechnical and Geoenvironmental Engineering*, 147 (11): 04021123. American Society of Civil Engineers.

Cekerevac, C., and L. Laloui. 2004. “Experimental study of thermal effects on the mechanical behaviour of a clay.” *Int J Numer Anal Methods Geomech*, 28 (3): 209–228. John Wiley & Sons, Ltd.

© ASCE

Coccia, C. J. R., and J. S. McCartney. 2016. “Thermal volume change of poorly draining soils I: Critical assessment of volume change mechanisms.” *Comput Geotech*, 80: 26–40. Elsevier.
Cui, Y. J., N. Sultan, and P. Delage. 2011. “A thermomechanical model for saturated clays.”
Fox, P. J., and T. B. Edil. 2011. “Effects of stress and temperature on secondary compression of peat.”
François, B., and L. Laloui. 2008. “ACMEG-TS: A constitutive model for unsaturated soils under non-isothermal conditions.” *Int J Numer Anal Methods Geomech*, 32 (16): 1955–1988. John Wiley & Sons, Ltd.
van Genuchten, M. T. 1980. “A Closed-form Equation for Predicting the Hydraulic Conductivity of Unsaturated Soils.” *Soil Science Society of America Journal*, 44 (5): 892–898. John Wiley & Sons, Ltd.
Grant, S. A., and A. Salehzadeh. 1996. “Calculation of Temperature Effects on Wetting Coefficients of Porous Solids and Their Capillary Pressure Functions.” *Water Resour Res*, 32 (2): 261–270. John Wiley & Sons, Ltd.
Hueckel, T., and G. Baldi. 1990. “Thermoplasticity of Saturated Clays: Experimental Constitutive Study.” *Journal of Geotechnical Engineering*, 116 (12): 1778–1796. American Society of Civil Engineers.
Hueckel, T., and M. Borsetto. 1990. “Thermoplasticity of Saturated Soils and Shales: Constitutive Equations.” *Journal of Geotechnical Engineering*, 116 (12): 1765–1777. American Society of Civil Engineers.
Lu, N. 2016. “Generalized Soil Water Retention Equation for Adsorption and Capillarity.” *Journal of Geotechnical and Geoenvironmental Engineering*, 142 (10): 04016051. American Society of Civil Engineers.
Lu, N., J. W. Godt, and D. T. Wu. 2010. “A closed-form equation for effective stress in unsaturated soil.” *Water Resour Res*, 46 (5): 5515. John Wiley & Sons, Ltd.
Lu, N., and W. J. Likos. 2006. “Suction Stress Characteristic Curve for Unsaturated Soil.” *Journal of Geotechnical and Geoenvironmental Engineering*, 132 (2): 131–142. American Society of Civil Engineers.
Mašín, D., and N. Khalili. 2012. “A thermo-mechanical model for variably saturated soils based on hypoplasticity.” *Int J Numer Anal Methods Geomech*, 36 (12): 1461–1485. John Wiley & Sons, Ltd.
Mccartney, J. S., N. H. Jafari, T. Hueckel, M. Sánchez, F. Vahedifard, J. S. Mccartney, N. H. Jafari, T. Hueckel, M. Sánchez, and F. Vahedifard. 2019. “Emerging Thermal Issues in Geotechnical Engineering.” 275–317. Springer, Cham.
Romero, E., A. Gens, and A. Lloret. 2001. “Temperature effects on the hydraulic behaviour of an unsaturated clay.” *Unsaturated Soil Concepts and Their Application in Geotechnical Practice*, 311–332. Springer, Dordrecht.
Romero, E., A. Gens, and A. Lloret. 2015. “Suction effects on a compacted clay under non-isothermal conditions.”
Salimi, K., A. B. Cerato, F. Vahedifard, and G. A. Miller. 2021. “Tensile Strength of Compacted Clays during Desiccation under Elevated Temperatures.” *Geotechnical Testing Journal*, 44 (4): 1119–1134. ASTM International.
Sultan, N., P. Delage, and Y. J. Cui. 2002. “Temperature effects on the volume change behaviour of Boom clay.” *Eng Geol*, 64 (2–3): 135–145. Elsevier.

© ASCE

Tang, A. M., and Y. J. Cui. 2011. “Controlling suction by the vapour equilibrium technique at different temperatures and its application in determining the water retention properties of MX80 clay.”

Tang, A. M., Y. J. Cui, and N. Barnel. 2008. “Thermo-mechanical behaviour of a compacted swelling clay.” *Geotechnique*, 58 (1): 45–54.

Vahedifard, F., T. D. Cao, E. Ghazanfari, and S. K. Thota. 2019. “Closed-Form Models for Nonisothermal Effective Stress of Unsaturated Soils.” *Journal of Geotechnical and Geoenvironmental Engineering*, 145 (9): 04019053. American Society of Civil Engineers.

Vahedifard, F., T. D. Cao, S. K. Thota, and E. Ghazanfari. 2018. “Nonisothermal Models for Soil–Water Retention Curve.” *Journal of Geotechnical and Geoenvironmental Engineering*, 144 (9): 04018061. American Society of Civil Engineers.

Xiong, Y., G. Ye, H. Zhu, S. Zhang, and F. Zhang. 2016. “Thermo-elastoplastic constitutive model for unsaturated soils.” *Acta Geotech*, 11 (6): 1287–1302. Springer Verlag.

Yavari, N., A. M. Tang, J. M. Pereira, and G. Hassen. 2016. “Effect of temperature on the shear strength of soils and the soil–structure interface.”

Ye, W. M., Y. W. Zhang, B. Chen, Z. J. Zheng, Y. G. Chen, and Y. J. Cui. 2012. “Investigation on compression behaviour of highly compacted GMZ01 bentonite with suction and temperature control.” *Nuclear Engineering and Design*, 252: 11–18. North-Holland.

Zhou, A. N., D. Sheng, S. W. Sloan, and A. Gens. 2012a. “Interpretation of unsaturated soil behaviour in the stress – Saturation space, I: Volume change and water retention behaviour.” *Comput Geotech*, 43: 178–187. Elsevier.

Zhou, A. N., D. Sheng, S. W. Sloan, and A. Gens. 2012b. “Interpretation of unsaturated soil behaviour in the stress–saturation space: II: Constitutive relationships and validations.” *Comput Geotech*, 43: 111–123.

© ASCE